UNIVERSITY OF TARTU

Faculty of Science and Technology

Institute of Chemistry

Verner Sääsk

Design of Highly Luminescent Anionic Manganese(II) Complexes for Application in Organic Light-Emitting Diodes

Master's thesis in Chemistry (30 ECTS)

Supervisors: Hou-Hsiu Chou, PhD

Kaija Põhako-Esko, PhD

Tartu 2023

ABSTRACT

Design of Highly Luminescent Anionic Manganese(II) Complexes for Application in Organic Light-Emitting Diodes

This study reports on the successful preparation of eight novel luminescent manganese(II) complexes, for which melting and degradation onset temperatures, X-ray diffraction patterns, luminescence spectra, emission lifetimes, and quantum yields were measured. Based on the results, $[BnMIm]_2[MnBr_4]$ (BnMIm = 1-benzyl-3-methylimidazolium ion) was chosen for the preparation of organic light-emitting diodes, due to its remarkable quantum yield ($\Phi = 0.59$) and high crystallinity. Next, to demonstrate applicability of complexes with $[BnMIm]^+$ cation as emitter materials, thin luminescent films were prepared out of them. Finally, optical band gap of $[BnMIm]_2[MnBr_4]$ was estimated from its absorption spectrum.

CERCS: P360 Inorganic chemistry; P395 Organometallic chemistry; P402 Photochemistry.

Keywords: inorganic chemistry, transition-metal complexes, manganese halides, lead-free perovskites, quantum yield, optoelectronics, organic light-emitting diode.

INFOLEHT

Kõrgluminestsentsete anioonsete mangaan(II) komplekside valmistamine orgaanilistes valgusdioodides kasutamiseks

Käesolevas töös valmistati kaheksa luminestsentset mangaan(II) kompleksi eesmärgiga töötada välja materjal orgaaniliste valgusdioodide jaoks. Sünteesitud kompleksidele mõõdeti nende sulamis- ja lagunemistemperatuurid, pulber röntgendifraktsiooni mustrid, luminestsents-spektrid, emissiooni eluajad ja absoluutsed kvantsaagised. Tulemusena leiti, et $[BnMIm]_2[MnBr_4]$ (BnMIm = 1-bensüül-3-metüülimidasooliumioon) on sobivaim kompleks orgaaniliste valgusdioodide valmistamiseks, selle väljapaistva kvantsaagise ($\Phi = 0{,}59$) ja kõrge kristallilisuse tõttu. Järgmisena, kompleksidest $[BnMIm]^+$ katiooniga valmistati õhukesed luminestsentsed kiled, et demonstreerida nende kasutatavust valgust kiirgava kihina. Lõpuks, $[BnMIm]_2[MnBr_4]$ optiline keelutsoon oli ligikaudselt määratud selle absorbtsiooni spektrist.

CERCS: P360 Anorgaaniline keemia; P395 Organometalliline keemia; P402 Fotokeemia.

Märksõnad: anorgaaniline keemia, üleminekumetallide kompleksid, mangaanhaliidid, pliivabad perovskiidid, kvantsaagis, optoelektroonika, orgaaniline valgusdiood.

CONTENTS

LIST OF ABBREVIATIONS USED

$[BzMIm]^+$	1-benzoyl-3-methylimidazolium ion
$[BnMIm]^+$	1-benzyl-3-methylimidazolium ion
$[cHMIm]^+$	1-cyclohexyl-3-methylimidazolium ion
$[EMIm]^+$	1-ethyl-3-methylimidazolium ion
$[Ph_4P]^+$	tetraphenylphosphonium ion
DBFDPO	4,6-bis(diphenylphosphoryl) dibenzofuran
DCM	dichloromethane
DMSO	dimethyl sulfoxide
DMF	dimethylformamide
DSC	differential scanning calorimetry
Eq	equivalent
EQE	external quantum efficiency
HOMO	highest occupied molecular orbital
LUMO	lowest unoccupied molecular orbital
MeCN	acetonitrile
MeOH	methanol
NA	not available
NMR	nuclear magnetic resonance
OLED	organic light-emitting diode
PPG-TDI	poly(propylene glycol) tolylene 2,4-diisocyanate
PXRD	powder X-ray diffraction
RT	room temperature
SC-XRD	single-crystal X-ray diffraction
TADF	thermally activated delayed fluorescence
TGA	thermogravimetric analysis
UV	ultraviolet

INTRODUCTION

It is hard to underestimate the impact climate change is having and will have on the quality of life on Earth [1,2]. To address the arising threat, changes are needed in all levels of human society [3], bust most importantly in the way we design, exploit and recycle materials and technologies.

One of the greatest technological innovations of the 21st century are organic light-emitting diodes (OLEDs) [4]. Being a key component of the contemporary displays, OLEDs are an economically crucial trend, with major electronic companies, such as LG, Samsung, Sony, and Apple actively increasing their OLED-based device portfolio [5–7]. Soon, OLEDs may take even bigger part of our lives, by being implemented in textiles or in electronic skin [8–10].

Despite its huge success, OLED technology has a significant flaw – commercially used OLEDs are currently designed to be nonreusable [11,12], which contributes a lot to a growing problem of electronic waste [13,14]. Furthermore, emitter materials used in OLEDs are more often than not based on rare metals, such as platinum [15,16] or iridium [17,18], making it hard to call OLED technology sustainable.

During last decade, an enormous amount of work had been done in order to develop cheaper, rare-metal free OLEDs, based on purely organic thermally activated delayed fluorescence (TADF) emitters [19,20]. However, most of developed TADF emitters are vulnerable to air [11], and potentially toxic [14], even further reducing recyclability of OLED technology. Therefore, it is clear that design of more environment-friendly OLEDs should be a high priority.

A promising solution for a new generation of OLED emitters are phosphorescent complexes, based on abundant transition-metals, such as iron(III) [21], tungsten(VI) [22,23] or manganese(II) [24,25] complexes. Especially manganese(II) complexes have attracted considerable interest very recently, due to their low cost and toxicity and features including bright phosphorescence, flexibility in molecular design and rich photofunctionality [26,27].

Motivated by the personal desire of contributing to the fight against climate change and inspired by the latest politico-economic initiatives, such as Green Transition in the European Union [28], this study focuses on developing intrinsically recyclable emitter materials for the use in OLED devices. As a molecular design strategy, anionic manganese(II) complexes with imidazolium-based counter cations were chosen. The ultimate aim of this work is to synthesize an anionic manganese(II) complex with an absolute quantum yield of at least 0.50 at room temperature.

1 LITERATURE OVERVIEW

1.1 Luminescence

Luminescence occurs when an excited molecule or atom relaxes to a lower energy state through emission of a photon [29]. Based on the mechanism of excitation, luminescence can be divided into bioluminescence (excitation via biochemical processes), electroluminescence (excitation via electric current), triboluminescence (excitation via physical stimuli), thermoluminescence (excitation via heating or cooling), but the most common is photoluminescence (excitation via absorption of light) [30]. When radiative relaxation to a ground state occurs without a change in electron spin ($S_1 \rightarrow S_0$), the phenomenon is termed fluorescence [31]; when initial and final states have different spins ($T_1 \rightarrow S_0$), term phosphorescence is used [31]. Fluorescence, a spin-allowed transition, is extremely fast process, which takes about 10^{-12} to 10^{-9} seconds to happen [32]; phosphorescence, a spin-forbidden transition, is noticeably slower, generally lasting from 10^{-6} to 10^{-3} seconds [32].

Common parameters used to characterize luminescent properties of materials are emission and excitation maxima, emission lifetime and absolute quantum yield [33].

Emission maxima are used to describe the color of the emission, while excitation maxima are useful to estimate energy levels of excited states [34,35]. Generally, emission maxima will have a redshift compared to excitation maxima, phenomenon discovered by Sir George Gabriel Stokes, and named after him [29]. Stokes shift is caused by non-radiative decay processes, such as vibrational relaxation, which can reduce the energy of an excited electron [36].

Emission lifetime is the mean time a molecule or an atom stays at an excited state before emitting a photon [36]. Since relaxation rates are significantly different for fluorescence and phosphorescence, it is possible to determine the luminescence mechanism of investigated compound by measuring its emission lifetime.

Luminescence absolute quantum yield (Φ), also known as quantum efficiency, describes the ratio between number of photons emitted and number of photons absorbed [31]:

$$\Phi = \frac{\text{Number of photons emitted}}{\text{Number of photons absorbed}} \quad (1)$$

Φ is a crucial parameter for the performance evaluation of luminescent materials [37]; for commercially used phosphors, Φ values close to 0.90 are typical [31]. A common way to estimate Φ of solids is by using integrating sphere apparatus, which collects all photons transmitted, scattered, and emitted by the sample [38].

1.2 Organic light-emitting diodes

OLEDs are electroluminescent devices which typically consist of six layers [12] (see Figure 1):

- cathode, made of conducting metals or their oxides, such as aluminum or zinc oxides.
- electron transport layer, which provides a pathway to electrons from the cathode.
- emissive layer, where electrons and holes recombine to create an exciton; radiative relaxation of exciton follows, giving rise to the electroluminescence phenomenon.
- hole transport layer, which provides a pathway to holes from the anode.
- anode, made of transparent conducting metal oxide, such as indium tin oxide.
- glass substrate, on which other layers are fixed.

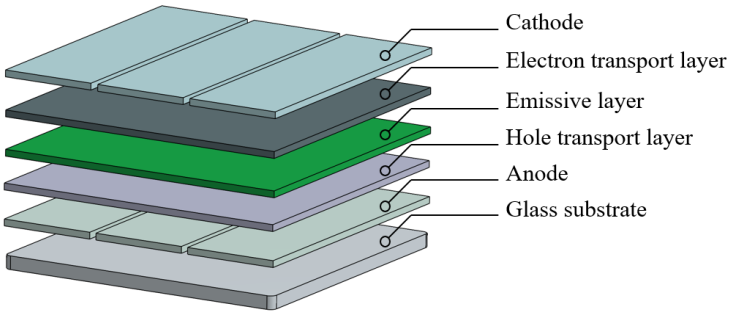

Figure 1. Schematic depiction of an OLED device.

Often, additional layers such as electron or hole injection layers are added, to reduce the barrier between work functions of cathodes or anodes and orbital energies of subsequent layers [12]. But the most crucial factor in achieving high efficiency in OLED devices is a rational design of the emissive layer [4]. Based on mechanism of the luminescence inside the emitters, three generations of OLED are commonly distinguished (see Figure 2 adopted from Volz *et al*. [12]).

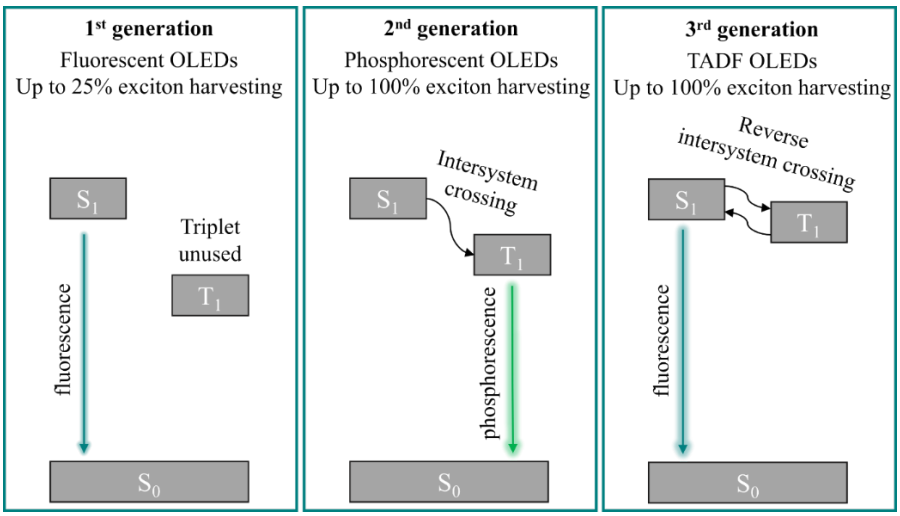

Figure 2. Luminescence mechanism inside OLED emitters of different generations.

1.2.1 First generation emitters

The first working OLED device was introduced in 1987 by Tang and Vanslyke [39]. As an emitter, they used fluorescent aluminum quinolate complex with a bright green emission [39]. Soon red and blue fluorescent emitters were designed [40,41], completing the first generation of fluorescent OLEDs. However, first generation emitters had an important intrinsic limitation. When electron and hole recombine inside the emitting layer, only about 25% of formed excitons will be in the singlet state, while about 75% will be in the triplet state [12]. As described before, for fluorescent systems, only transition of singlet excitons to the singlet ground state ($S_1 \rightarrow S_0$) is radiative, meaning that only 25% of the singlet excitons can be harvested for luminescence, while excitons in triplet state are unused (see Figure 2, left) [4]. Therefore, OLEDs with first generation emitters had a very low external quantum efficiencies (EQEs), prompting to a need of further research and development.

1.2.2 Second generation emitters

Next stage of the research focused on phosphorescent metal-organic emitters, with an aim to access remaining 75% of excitons in the triplet state. Phosphorescence was achieved by implementing heavy rare-metal atoms such as platinum [42] or iridium [43] into emitters. Presence of heavy atoms is needed to induce spin-orbit coupling, which facilitates intersystem crossing from singlet state to the triplet state ($S_1 \rightarrow T_1$) and accelerates radiative relaxation of the excitons from the triplet state to the singlet ground state ($T_1 \rightarrow S_0$) (see Figure 2, middle) [4].

Devices based on phosphorescent emitters showed good EQEs and allowed OLED technology to finally enter the display market [12]. However, despite the good efficiency of rare-metal based emitters, high fabrication price and uncertain toxicity of platinum and iridium complexes suggested that this technology is suitable only as a temporary solution and more generations of emitters are yet to come [44].

1.2.3 Third generation emitters

In 2012 an unexpected turn back to fluorescent OLEDs occurred, when Adachi *et al*. reported on a novel emission pathway via thermally activated delayed fluorescence (TADF) [20]. They demonstrated, that by carefully designing organic molecules for the emissive layer, even smaller energy gap (ΔE_{ST}) between S_1 and T_1 levels can be achieved [20]. This discovery was of a great importance, because for the molecules with a small ΔE_{ST}, the reverse intersystem crossing from T_1 to S_1 by thermal activation is possible, allowing to harvest the excitons from

the triplet state [44]. Emission eventually happens via radiative transition of singlet excitons to the singlet ground state ($S_1 \rightarrow S_0$), as in regular fluorescent emitters (see Figure 2, right).

Since then, for a decade, development of TADF emitters was a major trend in OLED research [44–46]. Contemporary TADF emitters exhibit excellent EQEs and emission lifetimes, as well as high luminance and color purity of the emission [47,48]. In addition, fabrication of organic TADF emitters is cheaper and relatively sustainable, since they are generally composed of abundant elements, such as carbon, nitrogen and oxygen [12]. Nevertheless, some researchers insist that further development of OLED emitters is necessary [4,12]. First of all, most of OLEDs based on TADF emitters are currently produced by vacuum thermal evaporation, which is energy and material consuming technique [12]. From economic perspective, solution processing (*e.g.* inkjet printing or spin coating), which can be done at ambient conditions, is preferable [49]. Furthermore, materials used in TADF emitters easily oxidize on air, which may produce potentially toxic compounds and hinder the recycling of OLED displays [14].

As possible fourth generation OLED emitters, a large variety of materials are currently being investigated. Some researchers focus on polymer emitters, aiming for applications in foldable and stretchable electronics [50,51], while others investigate combined TADF-fluorescent emitters [52–54] or metal-organic TADF emitters based on copper(I)-complexes [55–58], hoping to achieve even higher EQEs and color purity of the devices. Most recently, Mn(II) complexes have also attracted much attention as possible OLED emitters owing to their bright luminescence, low cost and toxicity, ease of synthesis, and, most importantly, their suitability for the solution processing [26,27].

1.3 Manganese(II) complexes

Photophysical properties of manganese(II) complexes were first systematically studied by Goodgame and Cotton in the early 1960s [59], and described in details by other researchers in the following decade [60–62]. It was determined that emission of Mn(II) complexes is of a phosphorescent nature and arises from the $^4T_1 \rightarrow {}^6A_1$ radiative transition (Figure 3, right) [59].

As illustrated by the Tanabe-Sugano diagram of a d^5 ion (see Figure 3, left), energy gap between $^6A_1$ and $^4T_1$ energy states decreases with an increase of crystal-field strength. Therefore, color of the emission is strongly dependent on the coordination environment of Mn(II) center [59]: for tetrahedral Mn(II) complexes, which have smaller crystal-field splitting parameter value, green emission color is characteristic, while for octahedral Mn(II) complexes with a larger crystal-field splitting parameter value, red emission color is common [59].

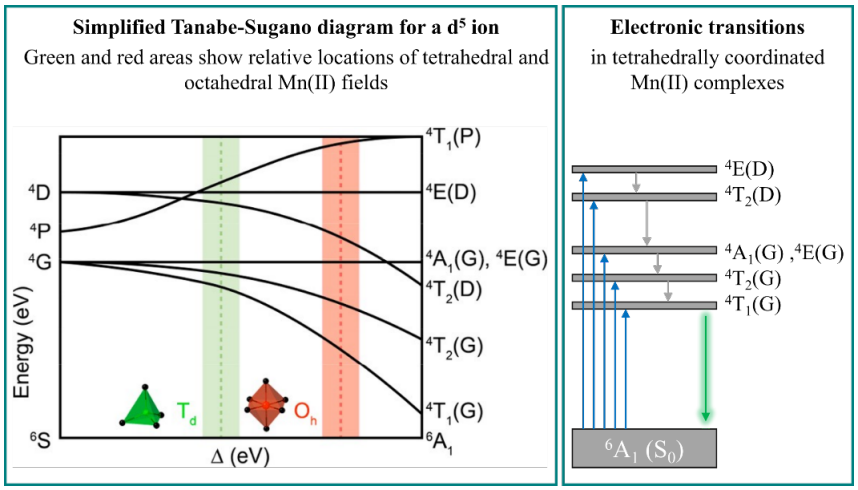

Figure 3. Tanabe-Sugano diagram for a d^5 ion reproduced from Morad *et al*. [63] (left) and schematic representation of electronic transitions in Mn(II) complexes (right).

Although luminescent manganese(II) complexes have been the subject of numerous studies since the work of Goodgame and Cotton, it was not until very recently when their potential for OLED application has been recognized and realized in the first device prototypes [26]. A pioneering work in this field was done by Xu *et al*. in 2017, when they reported on a successful fabrication of OLEDs based on an anionic tetrahedral Mn(II) complex, tetraphenyl-phosphonium tetrabromomanganate ($[Ph_4P]_2[MnBr_4]$, Figure 4, left) [24]. In their work, they used solution processing to fabricate devices with pure $[Ph_4P]_2[MnBr_4]$ as an emissive layer and with $[Ph_4P]_2[MnBr_4]$ doped into organic host materials, demonstrating that doped devices have superior EQE of 9.6% [24]. Different approach was taken by Qin *et al*. in 2019, when they used vacuum deposition to fabricate OLED emissive layers doped with a neutral manganese(II) complex, with 4,6-bis(diphenylphosphoryl) dibenzofuran and two bromine atoms as the ligands (DBFDPO-$MnBr_2$, Figure 4, right), which had even higher EQE of 10.5% [25].

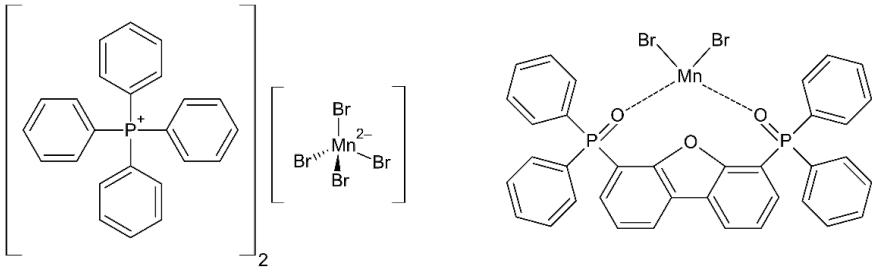

$[Ph_4P]_2[MnBr_4]$ **DBFDPO-$MnBr_2$**

Figure 4. First manganese(II)-based OLED emitters: $[Ph_4P]_2[MnBr_4]$ and DBFDPO-$MnBr_2$.

Inspired by the work of Xu *et al*. [24], current study focuses on anionic manganese(II) complexes, since they are more suitable for solution processing, an environment-friendly and economically feasible technique for OLED fabrication [12].

1.4 Anionic manganese(II) complexes

A key parameter to describe the suitability of luminescent compounds to be used as OLED emitters is their absolute photoluminescence quantum yield, Φ [4]. In case of anionic manganese(II) complexes, Φ depends on the structures of both anion and cation [26,27].

The majority of reported anionic manganese(II) complexes are homo-halomanganates ($[MnX_4]^{2-}$ or $[MnX_3]^-$; X represents a halogen atom), with chlorine [64–69], bromine [70–74] or iodine [75,76] atoms present as ligands. In addition to homo-halomanganates, mixed-halomanganates ($[MnX_2Y_2]^{2-}$; X and Y represent different halogen atoms) [76–78] and anions with other ligands, such as bis(trifluoromethanesulfonyl)amido ligand [79], were also reported. In case of halomanganates, complexes with bromine-containing anions generally have higher Φ compared to chlorine-containing anions [26], which is often associated with the larger spin-orbit coupling effect of the bromine atoms. Spin-orbit coupling effect of iodine atoms should be even larger due to their heavy mass, which theoretically may lead to a better Φ. Unfortunately, the information on Φ of homo- or mixed-iodomanganates is still too limited to confirm or overturn this theory [27]. However, it should be mentioned that lower Φ of complexes with iodine ligands compared to the ones with bromine ligands were reported before for some manganese(II) complexes [80,81]. This underlines the fact that Φ of manganese(II) complexes cannot be associated solely with spin-orbit coupling effect of the ligands. On the other hand, spin-orbit coupling unambiguously affects emission lifetime of the manganese(II) complexes, which decreases drastically when chlorine atoms are substituted with heavier bromine atoms and then decreases even more when iodine atoms are introduced [63,77].

Counter cations can affect the Φ of anionic manganese(II) complexes in multiple ways: by acting as a sensitizer for photon harvesting [27], by increasing the distance between manganese(II) centers [82] and by inducing the hydrogen bonding interactions with anion [71].

Since direct excitation from the ground state of manganese(II) center ($^6A_1$) to its excited states is spin-forbidden and thus not highly probable, absorption of isolated manganese(II) centers (*e.g.* in a solution) is rather small [63]. To increase photon harvesting of the system, it is important to add counter cations with a triplet energy level (T_1) slightly higher than the energy level of $^4A_1$, $^4E(G)$ excited state of Mn(II) center, which roughly equals to 2.9 eV [26]. This way, photons can be absorbed via spin-allowed $S_0 \rightarrow S_1$ transition in the organic counter cation, then transfer to its triplet state (T_1) via intersystem crossing, followed by another intersystem

crossing to the $^4A_1$, $^4E(G)$ state of Mn(II) center and non-radiative relaxation to its $^4T_1$ state, eventually relaxing to the $^6A_1$ ground state with the emission of photon.

As for the separation of manganese(II) centers, a strong correlation between the Mn···Mn distance and Φ was recently reported for both $[MnCl_4]^{2-}$ [83] and $[MnBr_4]^{2-}$ [82] anions, with complexes generally showing larger Φ when Mn···Mn distance is longer. Increased distance between manganese(II) centers seems to weaken the electronic interactions and non-radiative energy transfer between neighboring Mn atoms, which improves the Φ [83]. The same correlation should be true for complexes with $[MnI_4]^{2-}$ and mixed-halomanganate anions, as well as for tetrahedral Mn(II) complexes with other ligands. Therefore, when designing new luminescent anionic Mn(II) complexes, a bulky monovalent counter cations should be preferred, since they induce the separation of manganese(II) centers and thus improve the Φ.

Finally, it was reported by Gong *et al*. that hydrogen bonding between aliphatic C–H from counter cation and bromine from $[MnBr_4]^{2-}$ can improve rigidity of crystal structure, which reduces the thermal vibrations and thus suppresses the non-radiative transitions [71]. In their work, Gong *et al*. demonstrated that cation with five-membered pyrrolidinium is more sterically suitable for the formation of hydrogen bonds with anion, than six-membered piperidinium ring [71]. However, as demonstrated by Mao *et al*., hydrogen bonding can also decrease the Mn···Mn distance, which eventually leads to a smaller Φ [82]. Therefore, when choosing a counter cation which is capable of hydrogen bonding, it is especially important to functionalize it with bulky groups to avoid the unfavorable interaction between manganese(II) centers.

For the current study it was decided to focus on imidazolium-based counter cations, since they seem to satisfy all the described criteria. Imidazole is an aromatic system, which should have a high enough triplet energy level (T_1) for the intersystem crossing from counteraction to Mn(II) centers; imidazole is also a five membered ring, which should be sterically suitable for forming the hydrogen bonds with anions. Furthermore, luminescence of imidazolium-based Mn(II) complexes was reported before by Pitula and Mudring [79]. According to their work, introducing longer alkyl chains to imidazole ring lead to a decrease in crystallinity of the complexes, which resulted in a decrease of their luminescence intensity [79]. Therefore, bulky, but rigid groups were chosen to functionalize imidazole ring, in hope of improving the crystallinity of target complexes. Eventually, 1-ethyl-3-methylimidazolium ($[EMIm]^+$, which lead to the brightest emission in the work by Pitula and Mudring [79]), 1-benzyl-3-

methylimidazolium ([BnMIm]$^+$), 1-benzoyl-3-methylimidazolium ([BzMIm]$^+$) and 1-cyclohexyl-3-methylimidazolium ([cHMIm]$^+$) were selected as potential cations (Figure 5).

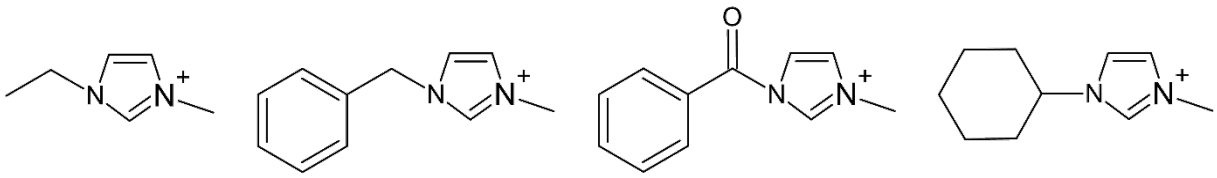

Figure 5. Imidazolium-based cations selected for the synthesis of manganese(II) complexes.

As anions it was decided to synthesize both homo- and mixed-halomanganates similarly to the work of Berezin *et al*. in 2021, when they have showed that mixed-halomanganates may have higher Φ compared to homo-halomanganates [76].

To study the effect of cations and anions on the luminescent properties of Mn(II) complexes, following workflow was designed:

1. Prepare six homo- and mixed-halomanganates from commercially available 1-ethyl-3-methylimidazolium salts: $[EMIm]_2[MnCl_4]$, $[EMIm]_2[MnBr_4]$, $[EMIm]_2[MnI_4]$, $[EMIm]_2[MnBr_2Cl_2]$, $[EMIm]_2[MnCl_2I_2]$ and $[EMIm]_2[MnBr_2I_2]$.
2. Select the anion which lead to the brightest luminescence among the [EMIm]$^+$-based complexes.
3. Synthesize necessary precursor salts to be used as a source of other counter cations: [BnMIm]X, [BzMIm]X and [cHMIm]X (X represents a halogen atom).
4. Synthesize three manganese(II) complexes with the most prominent anion and [BnMIm]$^+$, [BzMIm]$^+$ or [cHMIm]$^+$ used as the counter cations.
5. From the synthesized complexes, choose the counter cation which lead to the brightest luminescence. At last, synthesize five remaining halomanganates with chosen counter cation to compare them with [EMIm]$^+$-based complexes.

After the synthesis, structural, thermal and photophysical properties of prepared complexes were described in details to demonstrate their applicability as OLED emitters.

2 EXPERIMENTAL

Synthesis and physical measurements were conducted at Soft Functional Materials and Sustainable Energy Lab, Tsing Hua National University, Taiwan.

2.1 Physical measurements

^{1}H nuclear magnetic resonance (NMR) spectra were obtained using a Bruker AVANCE III HD 500 MHz apparatus. All spectra are presented on points per million (ppm) scale. Deuterated chloroform (chloroform-d), methanol (methanol-d_4) and dimethyl sulfoxide (DMSO-d_6) were purchased from Sigma-Aldrich Co. LLC.

For additional purity control, all final products were sent for analysis to the Elemental Analysis laboratory of National Chung Hsing University.

Single-crystal X-ray diffraction (SC-XRD) measurements were conducted on Rigaku XtaLAB Synergy R, DW system equipped with HyPix-Arc 150° detector. The crystals were kept at 100 K during data collection; as a radiation source Cu K_α (λ = 1.5418 Å) was used. Crystal structures were solved using olex2.solve [84] or SHELXT [85] structure solutions in Olex2 software [86]; refinement was conducted with SHELXL refinement package using least squares minimization [87]. Powder diffractograms were simulated from single crystal structures using Mercury software [88]. For powder X-ray diffraction (PXRD) measurements Bruker D2 PHASER diffractometer with Cu K_α (λ = 1.5418 Å) radiation source was used.

Simultaneous thermogravimetric analysis (TGA) and differential scanning calorimetry (DSC) were performed using a TA Instruments SDT-Q600 apparatus. Measurements were done in the range from room temperature to 400-500 °C under continuous nitrogen flow (0.1 L/min); scan rate was 1–10 °C/min, depending on the temperature region. Ceramic pans were used as a sample holder; Al_2O_3 powder was used as a reference.

2.2 Synthesis and single crystal growth

Sources of all reagents and solvents used can be found in Appendix 1. Structures of synthesized complexes are presented in Appendix 2; selected ^{1}H NMR spectra can be found in Appendix 3.

2.2.1 Synthesis of 1-ethyl-3-methylimidazolium-based complexes

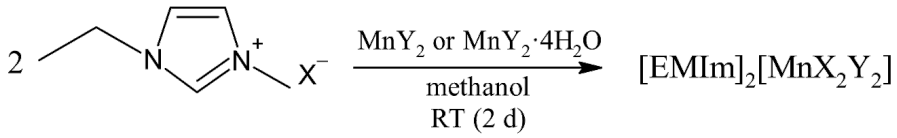

Figure 6. Synthesis of 1-ethyl-3-methylimidazolium-based halomanganates.

First, a series of manganese(II) complexes with 1-ethyl-3-methylimidazolium ($[EMIm]^{+}$) cation were synthesized following a route developed by Pitula and Mudring in 2010 (Figure 6), when they reported synthesis of $[EMIm]_2[MnCl_4]$ (**1a**), $[EMIm]_2[MnBr_4]$ (**1b**) and other similar compounds [79]. As reagents, commercially available 1-ethyl-3-methylimidazolium halides ([EMIm]X, X = Cl^-, Br^- or I^-) and anhydrous or hydrated manganese halides (MnY_2 or $MnY_2{\cdot}4H_2O$, Y = Cl^-, Br^- or I^-) were used.

For the synthesis, approximately 0.5 g of [EMIm]X was weighted into glass vials and dissolved in 10 mL of anhydrous methanol (MeOH). Then, stoichiometric amount of manganese halides was added into the vials (see Appendix 4 for details) and the mixtures were held in an ultrasonic bath (80 W, 40 kHz) until complete dissolution. Next, the vials were left to stir at room temperature (RT) for two days. Obtained solutions were then concentrated on rotary evaporator (50 °C, 10 torr), treated with diethyl ether (three times with 5 mL) and dried overnight *in vacuo*. As a result, $[EMIm]_2[MnCl_4]$ (**1a**), $[EMIm]_2[MnBr_4]$ (**1b**), $[EMIm]_2[MnBr_2Cl_2]$ (**1c**) and $[EMIm]_2[MnBr_2I_2]$ (**1e**) were obtained as luminescent green or orange solids, while $[EMIm]_2[MnI_4]$ and $[EMIm]_2[MnCl_2I_2]$ turned out to be black non-luminescent liquids.

The ^{1}H NMR analysis (methanol-d_4, 500 MHz, example spectra can be found in Appendix 3; analysis results are concluded in Appendix 5) had confirmed the purity of the luminescent compounds, but in case of $[EMIm]_2[MnI_4]$ and $[EMIm]_2[MnCl_2I_2]$ it showed that reactions had not occurred completely. Since only for the synthesis of $[EMIm]_2[MnI_4]$ and $[EMIm]_2[MnCl_2I_2]$ manganese iodide was used as a reagent, it seemed that its reactivity is somehow worse than that of manganese chloride or bromide. Different behavior of MnI_2 compared to other manganese halides was also reported before for the synthesis of tetraiodomanganates with tetrabutylammonium cation [89]. To confirm that source of the

problem was indeed MnI_2, the synthesis of $[EMIm][MnCl_2I_2]$ was repeated, but by using [EMIm]I and $MnCl_2$ as reagents instead. As anticipated, $[EMIm][MnCl_2I_2]$ (**1d**) synthesized in this way, turned out to be luminescent solid and consequent ^1H NMR analysis (Appendix 3) showed no traces of starting materials left. For the $[EMIm][MnI_4]$, the reaction was repeated with an excess of MnI_2, as suggested by Gill *et al*. [89], however, the product was still obtained as non-luminescent black liquid. Therefore, it was decided to omit the synthesis of $[MnI_4]^{2-}$ compounds and focus on five other halomanganates (see Figure 7).

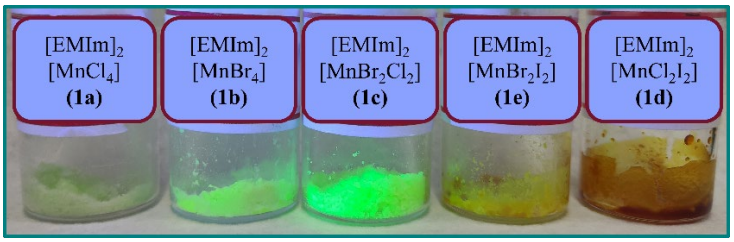

Figure 7. $[EMIm]^+$-based halomanganates upon irradiation with UV light.

Next, samples of all five synthesized compounds were sent for elemental analysis, which revealed that the purity of $[EMIm]_2[MnBr_4]$ (**1b**) and $[EMIm]_2[MnBr_2I_2]$ (**1e**) was lower compared to other samples, with carbon percentage being slightly larger than calculated values (see Appendix 5). Therefore, the synthesis of **1b** and **1e** was repeated with similar conditions and quantities, but with improved purification procedure: solutions were filtered through 0.45 µm filter after reaction and additional hexane wash was conducted after evaporation of solvent.

Samples of both compounds were then sent for elemental analysis once again, which revealed that additional purification had no noticeable effect: samples still exhibited heightened carbon percentage. Since **1b** and **1e** were both synthesized from $MnBr_2 \cdot 4H_2O$, which had slightly lower purity than other reagents (98% compared to 99% purity of $MnCl_2$), it is possible that high carbon percentage of samples may be caused by contamination with unreacted 1-ethyl-3-methylimidazolium halides. This assumption was then confirmed by ^1H NMR analysis, which showed no traces of other impurities in both samples (see Appendix 5). Since miniscule amount of unreacted 1-ethyl-3-methylimidazolium halides in samples should have negligible effect on their thermal and photophysical properties, it was decided that, despite fair results of elemental analysis, synthesized **1b** and **1e** were suitable for further measurements.

As illustrated by Figure 7, out of successfully synthesized $[EMIm]^+$-based halomanganates, $[EMIm]_2[MnBr_2Cl_2]$ (**1c**) showed brightest luminescence upon irradiation with 365 nm ultraviolet (UV) light. Surprisingly, luminescence intensity of **1d** and **1e** anions was rather low,

possibly due to their low crystallinity. Complexes **1d** and **1e** also turned out to be highly hygroscopic, making them hard to handle under ambient conditions. Therefore, out of synthesized novel $[EMIm]^+$-based halomanganates, only **1c** was determined to be suitable for the X-ray diffraction measurements. First, SC-XRD measurement was needed, to prove the structure of $[MnBr_2Cl_2]^{2-}$ anion. The crystals of **1c**, obtained from the synthesis route, were of perfect quality and hence were directly used for the SC-XRD measurement. Resulting diffractogram was successfully resolved (R_1 = 0.0266), proving anticipated structure of the complex (see Appendix 6). Next, PXRD measurement was conducted for powdered sample of **1c**, as well as for previously reported **1a** and **1b**. As structures of **1a** and **1b** were already reported before [79], and purity of those compounds was confirmed with other methods, it was decided that SC-XRD measurement is not necessary for them.

Next, to observe the influence of different organic counter cations on the luminescence intensity of complexes, an attempt to synthesize more compounds with $[MnBr_2Cl_2]^{2-}$ anion was made.

2.2.2 Synthesis of imidazolium halides: [BnMIm]Br, [BzMIm]Cl and [cHMIm]Cl

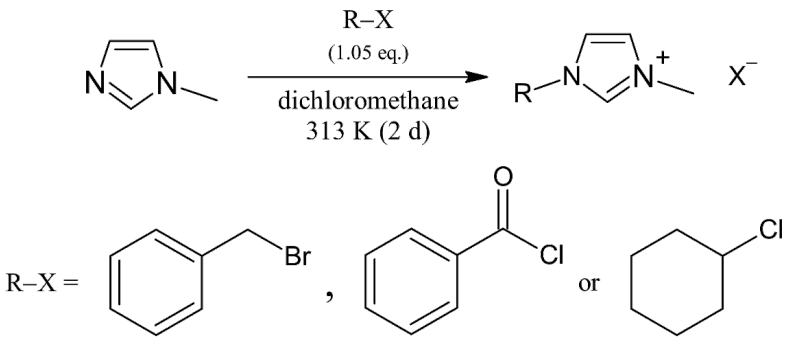

Figure 8. Synthesis of [BnMIm]Br, [BzMIm]Cl and [cHMIm]Cl.

Initially, benzylchloride, benzoylchloride and cyclohexylchloride were chosen as starting materials for the experiments, but arrival of the ordered benzylchloride was delayed, so it was replaced by benzylbromide, available at the laboratory chemical stock.

To synthesize target salts, a route from Shirota *et al*. was adopted (Figure 8) [90]. For all reactions, approximately 0.35 mL of 1-methylimidazole was dissolved in 5 mL of dichloromethane (DCM), then 1.05 equivalent of corresponding organic halide in 2 mL of DCM was added dropwise (see Appendix 7 for details). Resulting solutions were then left to stir under reflux for two days. Finally, solutions were concentrated on rotary evaporator (50 °C, 10 torr) and dried overnight *in vacuo*.

For the [BnMIm]Br and [BzMIm]Cl described synthesis route resulted in slightly heightened yields, 110% and 114% accordingly, which can be attributed to the leftovers of solvent or absorbed water. On the other hand, in case of [cHMIm]Cl the reaction yielded in only 35% of theoretical amount.

The ^{1}H NMR measurement (chloroform-d, 500 MHz, see spectra in Appendix 3 and analysis results in Appendix 8) confirmed the structures of [BnMIm]Br and [BzMIm]Cl, however for the hypothetical [cHMIm]Cl it showed that sample consisted almost exclusively of 1-methylimidazole, indicating that no reaction occurred, and thus explaining the low yield.

It was then decided to repeat the synthesis of [cHMIm]Cl under higher temperature, aiming to promote the substitution reaction. To do so, the reaction was conducted with the same quantities of starting materials, but in acetonitrile (MeCN) under reflux (T = 80 °C). However, almost identically low yield of 38% was achieved. Eventually, it was concluded that the reactivity of secondary halide group in cyclohexylchloride is too low for the desired substitution reaction and the synthesis of [cHMIm]Cl was put on hold. In the future, similar reaction may be attempted with more reactive cyclohexylbromide or by using a primary halide, such as cychlohexylmethylchloride, instead.

For the [BnMIm]Br and [BzMIm]Cl compounds it was concluded based on NMR analysis that samples are of satisfying purity to be used for further reactions.

Synthesis of [BnMIm]Br was later repeated on a larger scale (see Appendix 7) and a diethyl ether wash (three times with 5 mL) before drying, resulting in a more reasonable yield of 97%.

2.2.3 Synthesis of $[BnMIm]_2[MnBr_2Cl_2]$ and $[BzMIm]_2[MnBr_2Cl_2]$

To prepare $[BnMIm]_2[MnBr_2Cl_2]$ and $[BzMIm]_2[MnBr_2Cl_2]$, organic precursor salts were dissolved in methanol, then stoichiometric amount of $MnCl_2$ or $MnBr_2 \cdot 4H_2O$ was added (see Appendix 9 for details), and resulting solutions were left to stir at RT for two days. Next, samples were concentrated on rotary evaporator (50 °C, 10 torr) and dried *in vacuo* overnight, resulting in 0.2938 g (96% yield) and 0.3457 g (92% yield) of $[BnMIm]_2[MnBr_2Cl_2]$ and $[BzMIm]_2[MnBr_2Cl_2]$ accordingly. Interestingly, while $[BnMIm]_2[MnBr_2Cl_2]$ showed bright green luminescence upon irradiation with 365 nm UV light, $[BzMIm]_2[MnBr_2Cl_2]$ turned out to be completely non-luminescent. Absence of luminescence in $[BzMIm]_2[MnBr_2Cl_2]$ may be attributed to the effect of oxygen atom from benzoyl group, which can possibly bond to manganese center and open additional non-radiative relaxation pathway. Another explanation

is that reaction simply did not occur and luminescent $[MnBr_2Cl_2]^{2-}$ anion was not formed. Since obtained ^1H NMR spectra (methanol-d_4, 500 MHz, see Appendix 3 and Appendix 10) for both compounds corresponded to expected structures and showed no significant impurities, it was decided to conduct more precise structure control via SC-XRD. Since crystals of obtained from described reaction route were too small, next stage of experiments focused on preparation of single crystals of $[BnMIm]_2[MnBr_2Cl_2]$ and $[BzMIm]_2[MnBr_2Cl_2]$.

2.2.4 Single crystal growth of $[BnMIm]_2[MnBr_2Cl_2]$ and $[BzMIm]_2[MnBr_2Cl_2]$

To obtain high-quality single crystals, gradual concentration growth of crude solution is required. For the first recrystallization experiment, antisolvent vapor assisted crystallization method was chosen as an established way to produce large single crystals for organic metal halides [67,91]. In case of antisolvent vapor assisted crystallization, the concentration grow is achieved through slow diffusion of antisolvent vapors into the solvent.

Based on a series of solubility tests, methanol and diethyl ether were chosen as solvent and antisolvent accordingly. For recrystallization, a spatula full of $[BnMIm]_2[MnBr_2Cl_2]$ or $[BzMIm]_2[MnBr_2Cl_2]$ was transferred to 5 mL glass vials, dissolved in 300 µL of anhydrous methanol and held in ultrasonic bath (80 W, 40 kHz) for five minutes. Then, 5 mL vials with the precursor solutions were put into larger, 50 mL vials. Finally, 3 mL of diethyl ether was added to the 50 mL vials, and closed vials were left at RT for a week (see Figure 9, left).

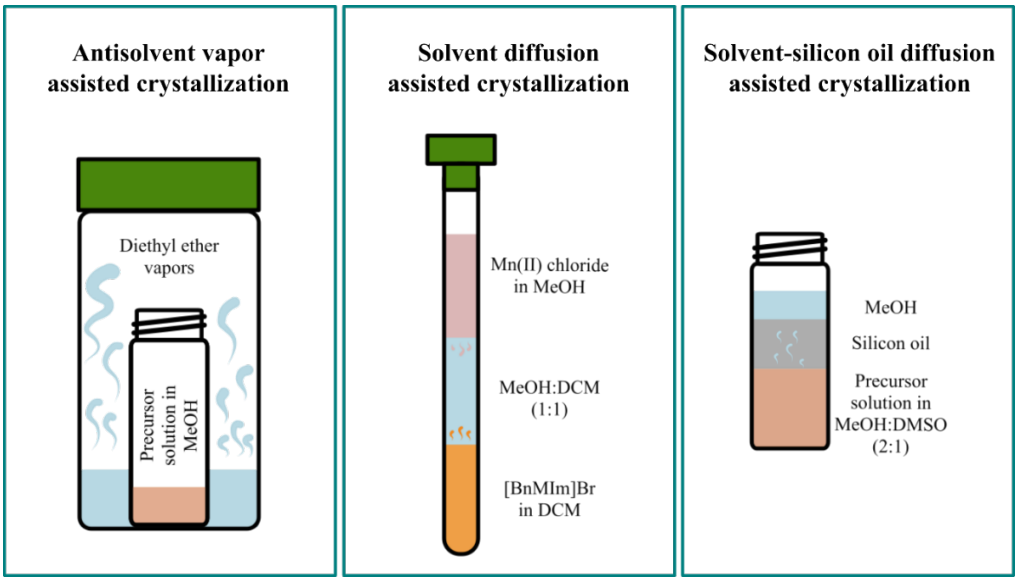

Figure 9. Different methods used for the growth of single crystals.

After a week, some crystallization was observed for both compounds. Obtained crystals of $[BnMIm]_2[MnBr_2Cl_2]$ were rather small, but brightly luminescent. On the other hand, for the

assumed $[BzMIm]_2[MnBr_2Cl_2]$, two different set of crystals formed: yellow (most probably [BzMIm]Cl) and pinkish white (most probably $MnBr_2 \cdot 4H_2O$ or $MnBr_2$), indicating that no reaction occurred. This was later confirmed by elemental analysis (see Appendix 10), which showed significantly different composition from the calculated values for assumed $[BzMIm]_2[MnBr_2Cl_2]$. Therefore, the addition of benzoyl group to imidazole ring probably had a negative impact on the reactivity of the imidazolium salt. To understand the reasons of this influence, similar reaction may be repeated under higher temperature or in different solvent and potentially studied *in silico* in the future.

2.2.5 Liquid diffusion assisted crystal growth of $[BnMIm]_2[MnBr_2Cl_2]$

Since quality of $[BnMIm]_2[MnBr_2Cl_2]$ crystals obtained from antisolvent vapor assisted crystallization method had left more to be desired, it was decided to continue recrystallization experiments, by testing two different liquid diffusion assisted crystallization methods.

For the first approach, starting materials for $[BnMIm]_2[MnBr_2Cl_2]$ synthesis were dissolved in two solvents with different density, while maintaining a stoichiometric ratio for the reaction; [BnMIm]Br dissolved in DCM (ρ = 1.33 g/cm^3) and $MnCl_2$ in MeOH (ρ = 0.79 g/cm^3). Resulting solutions were transferred to a long glass tube as follows: first a layer of [BnMIm]Br solution in DCM, next a layer of DCM:MeOH (1:1) mixture and finally a layer of $MnCl_2$ solution in MeOH. Closed tube was then left to diffuse at RT for a week (see Figure 9, middle).

Another liquid diffusion assisted crystallization method for preparation of high-quality single crystals was recently suggested by Yao *et al*. [91]. They claimed that by adding a layer of silicone oil on top of the precursor solution, a controlled concentration growth, limited by the diffusion of solvent molecules through the silicone oil, can be achieved (Figure 9, right) [91]. It is important to notice that solvents used for this approach must be lighter than silicon oil (ρ = 0.971 g/cm^3), and also capable of diffusing through it. In their work Yao *et al*. had suggested 1:1 dimethylformamide (DMF):DMSO mixture as one of the suitable solvent systems, in which DMF (ρ = 0.944 g/cm^3) acts as the escaping solvent [91]. Furthermore, they have demonstrated that precursor solutions with concentrations around 0.25–0.5 M result in higher crystallization yields [91].

In current study, MeOH:DMSO (2:1) solvent system was selected, since $[BnMIm]_2[MnBr_2Cl_2]$ was found to be insoluble in DMF. Methanol has low density (ρ = 0.792 g/cm^3) and very high polarity, therefore it should easily diffuse through the silicon oil, providing necessary concentration growth of the precursor solution. To grow the crystals, 0.3445 g (1.36 mmol) of

[BnMIm]Br and 0.0859 g (0.68 mmol) $MnCl_2$ was weighted into 5 mL vial and dissolved in 2.25 mL of selected solvent system (1.50 + 0.75 mL of MeOH and DMSO accordingly) to form a ~0.3 M solution. Next, approximately 1 mL of silicon oil was slowly added on top of the solution and the vial was left at RT for a week.

After a week, no crystal formation was observed in both crystallization systems. When another week passed without any significant changes, it was decided to reduce the amount of silicon oil in the second system, to increase the rate of methanol escape and thus promote the crystallization. However, still no crystals appeared. Therefore, it may be speculated that $[BnMIm]_2[MnBr_2Cl_2]$ is too soluble in methanol and antisolvent presence is required to obtain the crystals. Alternatively, other polar solvents like ethanol, isopropanol or acetonitrile may be tested for liquid diffusion assisted crystallization in the future.

Since none of the liquid diffusion assisted crystallization methods eventually succeeded, crystals of $[BnMIm]_2[MnBr_2Cl_2]$, obtained from antisolvent vapor assisted crystallization method were used for SC-XRD measurement. As expected, measurement resulted in a rather high *R*-factor ($R_1 = 0.1028$), however it was still possible to resolve the structure (Appendix 6), providing yet another proof for the successful synthesis of $[BnMIm]_2[MnBr_2Cl_2]$.

Next, remaining halomanganates with $[BnMIm]^+$ counter cation were synthesized to compare their luminescent properties with $[EMIm]^+$-based compounds.

2.2.6 Synthesis of imidazolium halides II: [BnMIm]Cl and [BnMIm]I

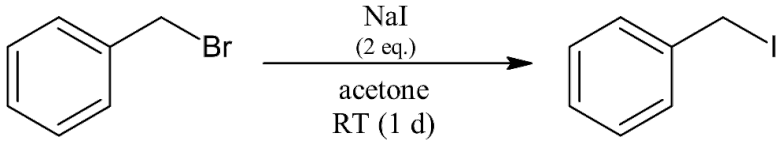

Figure 10. Synthesis of benzyliodide via Finkelstein reaction.

While still waiting for benzylchloride to arrive, benzyliodide was synthesized via Finkelstein reaction from benzylbromide (Figure 10). For this reaction, 1.8399 g (12.28 mmol) of sodium iodide was dissolved in 8 mL of acetone in a 50 mL glass flask, then 0.74 mL (6.23 mmol) of benzylbromide dissolved in 2 mL of acetone was added dropwise and the flask was left to stir at RT overnight. Next day, 15 mL of saturated NaCl solution was added to reaction flask and resulting mixture was transferred to a separating funnel. The mixture was then extracted thrice with 5 mL of diethyl ether; organic phases were combined, dried over $MgSO_4$, concentrated on rotary evaporator (40 °C, 10 torr) and dried overnight *in vacuo*, resulting in 1.1508 g

(85% yield) of orange-brown solid, benzyliodide. Subsequent ^{1}H NMR analysis (chloroform-d, 500 MHz, see Appendix 3) confirmed the structure and purity of synthesized compound.

Shortly after synthesis of benzyliodide, ordered benzylchloride arrived and both halides were reacted with 1-methylimidazole under the conditions described before (see Figure 8 and Appendix 7 for details), resulting in 1.3923 g (83% yield) of [BnMIm]Cl and 1.2556 g of [BnMIm]I (104% yield; high value could be attributed to the absorbed water). Based on ^{1}H NMR analysis (DMSO-d_6 and chloroform-d accordingly, 500 MHz, see Appendix 8), both compounds were determined to be of a suitable purity for further reactions.

2.2.7 Synthesis of 1-benzyl-3-methylimidazolium-based complexes

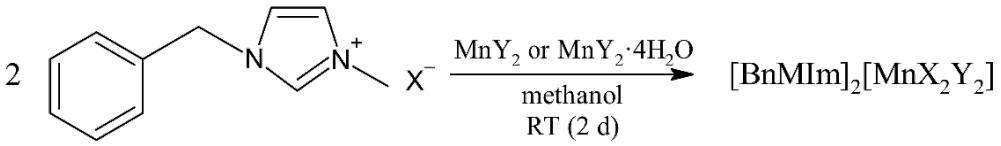

Figure 11. Synthesis of 1-benzyl-3-methylimidazole-based halomanganates.

Finally, $[BnMIm]_2[MnCl_4]$ (**2a**), $[BnMIm]_2[MnBr_4]$ (**2b**), $[BnMIm]_2[MnBr_2Cl_2]$ (**2c**, reaction was repeated on a larger scale), $[BnMIm]_2[MnCl_2I_2]$ (**2d**) and $[BnMIm]_2[MnBr_2I_2]$ (**2e**) were synthesized under the same conditions as $[EMIm]^+$-based compounds (see Figure 11 and Appendix 9 for details), resulting in green or orange luminescent solids. As decided previously, MnI_2 was not used for reactions and hence synthesis of $[BnMIm]_2[MnI_4]$ was not attempted.

The ^{1}H NMR spectra (methanol-d_4, 500 MHz, see Appendix 11) of all five compounds corresponded to expected structures and subsequent elemental analysis (Appendix 11) showed good purity of samples. **2b** and **2e**, synthesized from $MnBr_2·4H_2O$, showed slightly heightened carbon percentage, but it was decided that their purity is also within acceptable limits.

Similarly to the $[EMIm]^+$-based compounds, **2d** and **2e** turned out to be highly hygroscopic compounds with low crystallinity. Therefore, PXRD measurement was possible only for complexes **2a**–**2c**. In addition, powder diffractograms of $MnCl_2$ or $MnBr_2·4H_2O$ were recorded for the comparison. Finally, an attempt to prepare single crystals of **2a** and **2b** was made via antisolvent vapor assisted crystallization method, similarly to the procedure described above. For both **2a** and **2b** some crystal formation was achieved, but consequent SC-XRD measurement showed that quality of obtained crystals was insufficient to resolve the structures of the complexes. In the future, more work should be done to develop suitable single crystal growth method for imidazolium-based anionic manganese(II) complexes.

2.3 Photophysical measurements

After confirming the structures and purity of synthesized complexes **1a**–**1e** and **2a**–**2e**, their photophysical properties were investigated, by measuring luminescence spectra, emission lifetime, and Φ at RT.

For complex **2b**, UV-visible absorption spectrum in solid state was also measured using JASCO V-650 spectrophotometer equipped with a photomultiplier tube detector.

2.3.1 Luminescence spectra

Luminescence spectra were recorded using Hitachi F-2500 Fluorescence Spectrophotometer with a 150W xenon lamp excitation light source. Optimal excitation wavelengths were chosen based on test measurements; optimal emission wavelengths were derived from the emission maxima.

2.3.2 Luminescence quantum yield

Luminescence quantum yield (Φ) measurements were conducted in collaboration with Kwansei Gakuin University, Japan. For the measurements Hamamatsu Photonics C9920-02 system equipped with an integrating sphere apparatus and a 150 W CW xenon light source was used. The accuracy of the instrument was confirmed by measuring the Φ value of the reference, anthracene in ethanol (Φ = 0.27) [92].

2.3.3 Luminescence emission lifetime

Emission lifetime measurements were conducted at the estimated excitation maxima of samples using the Edinburgh FLS980 instrument, equipped with a xenon microsecond flashlamp (μF2).

Obtained emission decay curves were analyzed with both single- and bi-exponential models, giving preference to the fitting with better χ^2 result to calculate the emission lifetime values. If single-exponential model resulted in a better fitting, pre-exponential factors (A_0) and emission lifetimes (τ_0) were obtained from Equation 1:

$$I(t) = A_0 \cdot \exp(-t/\tau_0), \quad (1)$$

For bi-exponential model, pre-exponential factors (A_1 and A_2) and average emission lifetimes (τ_{av}) were calculated from Equation 2:

$$\tau_{av} = \frac{A_1\tau_1^2 + A_2\tau_2^2}{A_1\tau_1 + A_2\tau_2}, \quad (2)$$

3 RESULTS AND ANALYSIS

In 2017 Xu *et al*. reported on fabrication of green-light-emitting OLED based on anionic Mn(II) complex with tetraphenylphosphonium cation [24], however, since then application of similar complexes in OLEDs was very limited [25]. This study aimed to continue the route started by Xu *et al*. by focusing on anionic halomanganates, and their application in OLEDs. In total, ten imidazolium-based Mn(II) complexes were synthesized, of which eight are novel compounds. For synthesized complexes, crystal structures (if possible), as well as thermal and photophysical properties, such as melting points, thermal stability windows, luminescence spectra, emission lifetimes and Φ, were described in details. In addition, UV-visible absorption spectra, as well as the luminescence in polymer matrix were recorded for selected compounds, to explore their applicability in optoelectronic devices.

3.1 X-ray diffraction analysis

Of all synthesized compounds, only single crystals of **1c** and **2c** were of satisfying quality for SC-XRD measurements. For them, average Mn···Mn distances were estimated from the obtained crystal structures (see Appendix 6). As expected, average distances between Mn(II) centers in **2c** were longer, than in **1c** (10.31 Å against 8.30 Å), demonstrating the influence of a bulky benzyl group on a crystal structure of the Mn(II) anionic complexes.

Next, for complexes **1c** and **2c**, powder X-ray diffractograms were simulated based on their crystal structures and compared to the data obtained from PXRD measurements (Figure 12).

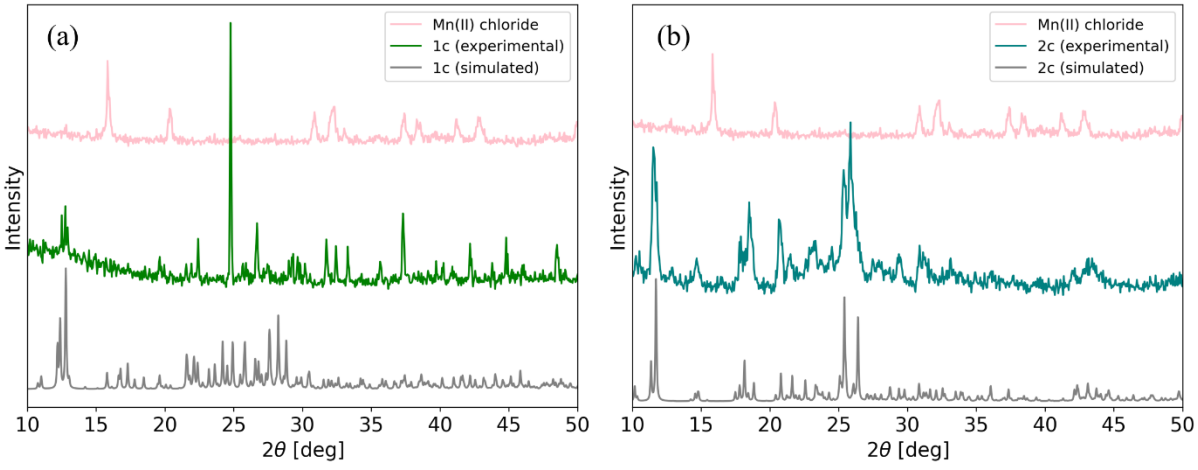

Figure 12. Diffractograms of **1c** (a) and **2c** (b); crude $MnCl_2$ data plotted for reference.

As can be seen from the Figure 12, the experimental data is in a good agreement with the simulation, providing yet another proof for the correct structure of **1c** and **2c**. Diffractograms of complexes **1c** and **2c** also demonstrated that both imidazolium-based complexes show

similar crystal structures, with the most intense peaks located at 2θ values of 10–15 degrees and 25–30 degrees, which are absent in the starting material, $MnCl_2$. It is also important to notice that there are no signals of characteristic peak of $MnCl_2$ (2θ = 15.8) in diffractograms of complexes **1c** and **2c**, indicating that no traces of starting material are left in the samples.

As mentioned before, iodine ligand containing complexes **1d**–**1e** and **2d**–**2e** were too hygroscopic and rapidly lost their crystallinity at ambient conditions, therefore PXRD measurements for those complexes was obstructed. PXRD diffractograms of other complexes, **1a**–**1b** and **2a**–**2b**, show almost identical peak fingerprints to the ones observed in experimental and simulated diffractograms of **1c** and **2c** accordingly (see Figures 12 and 13).

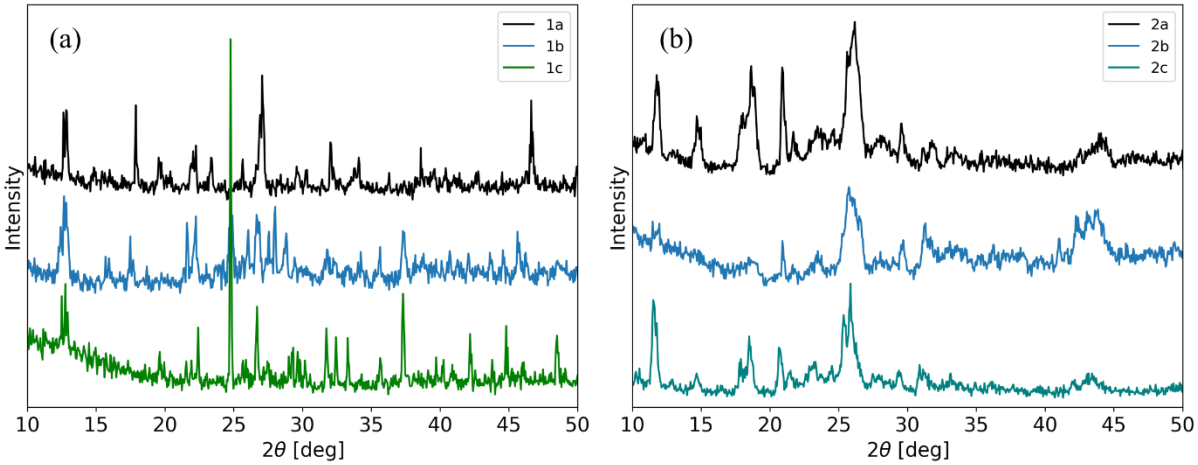

Figure 13. PXRD diffractograms of complexes **1a**–**1c** (a) and **2a**–**2c** (b).

From obtained diffractograms it seems that influence of halide ligands on crystal structures of imidazolium-based hybrid halomanganates is marginal and the largest differences arise from counter cations.

XRD analysis provided more evidence for the correct structure and purity of synthesized complexes. In the future, crystal structures of **1c** and **2c**, obtained from SC-XRD measurement, will be used to calculate energies of excited states of $[MnBr_2Cl_2]^{2-}$ anion *in silico*.

Next, thermal properties of synthesized complexes **1a**–**1e** and **2a**–**2e** were studied via simultaneous TGA/DSC measurement.

3.2 Thermal properties

Raw data from simultaneous TGA/DSC measurements was processed in the Universal Analysis, a software provided by TA Instruments (see fitting examples in Appendix 12). Melting points (T_m), obtained from endothermic peaks of DSC curves (Figure 14), and degradation onset temperatures (T_o), extrapolated from TGA curves (Figure 15) are concluded in Table 1.

Table 1. Melting points and degradation onset temperatures of neat **1a**–**1e** and **2a**–**2e**.

Complex	T_m[a] (°C)	T_o[b] (°C)
$[EMIm]_2[MnCl_4]$ (**1a**)	78	326
$[EMIm]_2[MnBr_4]$ (**1b**)	59	340
$[EMIm]_2[MnBr_2Cl_2]$ (**1c**)	60	318
$[EMIm]_2[MnCl_2I_2]$ (**1d**)	45	309
$[EMIm]_2[MnBr_2I_2]$ (**1e**)	48	317
$[BnMIm]_2[MnCl_4]$ (**2a**)	128	298
$[BnMIm]_2[MnBr_4]$ (**2b**)	132	311
$[BnMIm]_2[MnBr_2Cl_2]$ (**2c**)	135	278
$[BnMIm]_2[MnCl_2I_2]$ (**2d**)	93	252
$[BnMIm]_2[MnBr_2I_2]$ (**2e**)	98	271

[a]T_m: melting point. [b]T_o: degradation onset temperature.

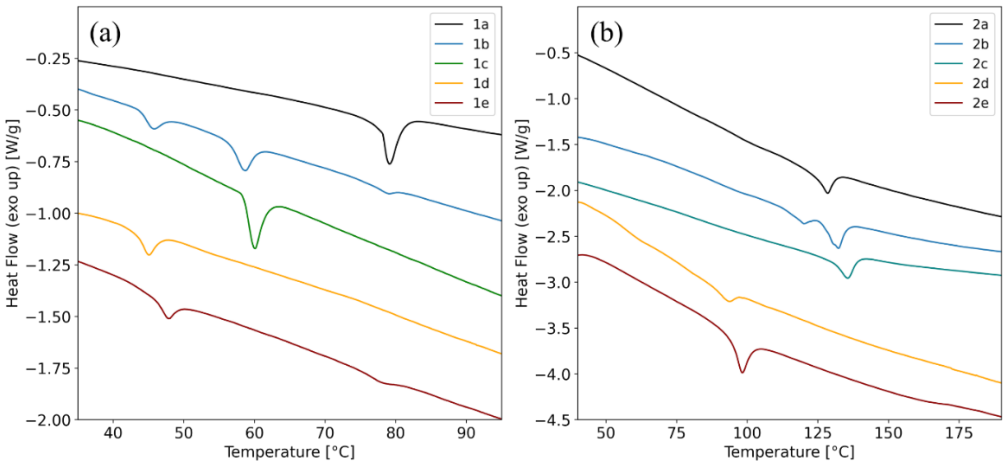

Figure 14. DSC curves of complexes **1a**–**1e** (a) and **2a**–**2e** (b).

As can be seen from Table 1 and Figure 14, melting points of $[BnMIm]^+$-based compounds are significantly higher than melting points of $[EMIm]^+$-based compounds. This is logical, since

addition of benzyl group should lead to a higher crystallinity of structures, caused by aromatic π-stacking. This type of interaction can indeed be observed in crystal structure of complex **2c**, obtained from SC-XRD measurement (see Appendix 6), where imidazole rings are positioned in parallel with benzyl rings, clearly indicating presence of the π-orbital interaction between two aromatic systems.

Interestingly, in case of complex **1b**, two peaks can be observed on the DSC curve. Most probably, weaker peak at approximately 46 °C can be attributed to solid-solid phase transition, which was reported before for this complex [93]. Another important point to mention is that measured melting point of **1b** (T_m = 59 °C) is somewhat different from the melting point value of 72 °C, reported for this complex by Pitula and Mudring in 2010 [79]. To double check the obtained result, TGA/DSC measurement was repeated for another batch of complex **1b**. Nevertheless, same result of T_m = 59 °C was obtained. One possible explanation of lower melting point can be attributed to high hygroscopicity of complex **1b**, which could potentially lead to a formation of hydrates with lower melting points. Even though all samples were thoroughly vacuumed before measurements, high air humidity of Taiwan could have a negative impact on the results. Therefore, for complex **1b**, more precise DSC measurement, conducted with a sample prepared inside the glove box and sealed in hermetic aluminum pan should be done in the future.

As for the TGA measurements, synthesized complexes exhibited good thermal stability, showing little or no degradation at temperatures as high as 250 °C (see Figure 15). This is of a great significance for emitter materials, since fabrication and workflow of optoelectronic devices are often associated with high temperatures [70].

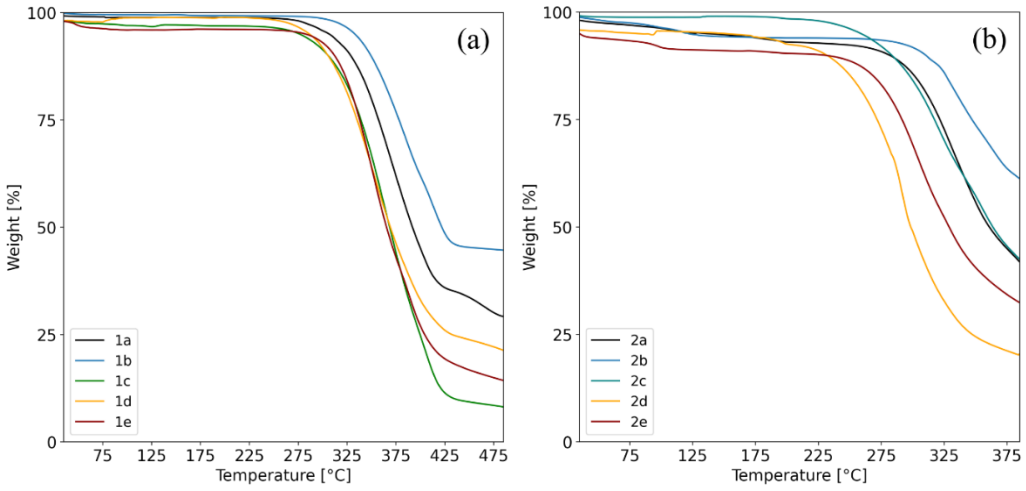

Figure 15. TGA curves of complexes **1a**–**1e** (a) and **2a**–**2e** (b).

Comparing Figures 14 and 15, it can be noticed that despite having higher melting points, $[BnMIm]^+$-based compounds have lower thermal stability compared to $[EMIm]^+$-based compounds, which is a slightly counterintuitive result. One possible explanation of this result is that electron-accepting properties of benzene ring significantly reduce charge density on adjacent carbon atom, resulting in a weaker covalent bonding between this carbon and nitrogen from the imidazole ring. In this case, interaction of benzyl group with imidazole ring should be weaker than that of the ethyl group, resulting in a lower thermal stability of compounds with $[BnMIm]^+$ cation.

The TGA/DSC measurements strongly indicate that synthesized complexes have suitable thermal properties to be applied in various light-emitting devices. Low melting points of synthesized complexes can facilitate film fabrication through simple melting-recrystallization procedure, while wide thermal stability window can ensure that light-emitting layer would not decompose during fabrication or exploitation of the devices.

3.3 Photophysical properties

Results of conducted photophysical measurements are concluded in a Table 2.

Table 2. Photophysical data of neat **1a**–**1e** and **2a**–**2e** at room temperature.

Complex	$\lambda_{ex}^{max,\,1}$ (nm)	$\lambda_{ex}^{max,\,2}$ (nm)	λ_{em}^{max} (nm)	Φ[a]	τ[b] (ms)
$[EMIm]_2[MnCl_4]$ (**1a**)	363	452	527	0.06	0.71
$[EMIm]_2[MnBr_4]$ (**1b**)	363	452	513	0.47	0.58
$[EMIm]_2[MnBr_2Cl_2]$ (**1c**)	376	451	515	0.36	0.71
$[EMIm]_2[MnCl_2I_2]$ (**1d**)	383	489	539	NA[c]	NA
$[EMIm]_2[MnBr_2I_2]$ (**1e**)	381	470	536	NA	NA
$[BnMIm]_2[MnCl_4]$ (**2a**)	360	450	531	0.23	2.67
$[BnMIm]_2[MnBr_4]$ (**2b**)	364	453	516	0.59	0.58
$[BnMIm]_2[MnBr_2Cl_2]$ (**2c**)	364	454	524	0.28	0.64
$[BnMIm]_2[MnCl_2I_2]$ (**2d**)	378	488	540	NA	NA
$[BnMIm]_2[MnBr_2I_2]$ (**2e**)	375	489	537	0.01	NA

[a]Φ: emission quantum yield. [b]τ: emission lifetime.
[c]NA: not available, because of too low luminescence intensity.

3.3.1 Luminescence spectra

As can be seen from Figure 16, all complexes had almost identical shape of emission curves, with a strongest emission at a wavelength interval of 500–550 nm, *i.e.* green emission. This is an anticipated result, since emission of synthesized complexes should arise solely from $^4T_1 \rightarrow {}^6A_1$ radiative transition, characteristic for tetrahedral Mn(II) complexes [26,27].

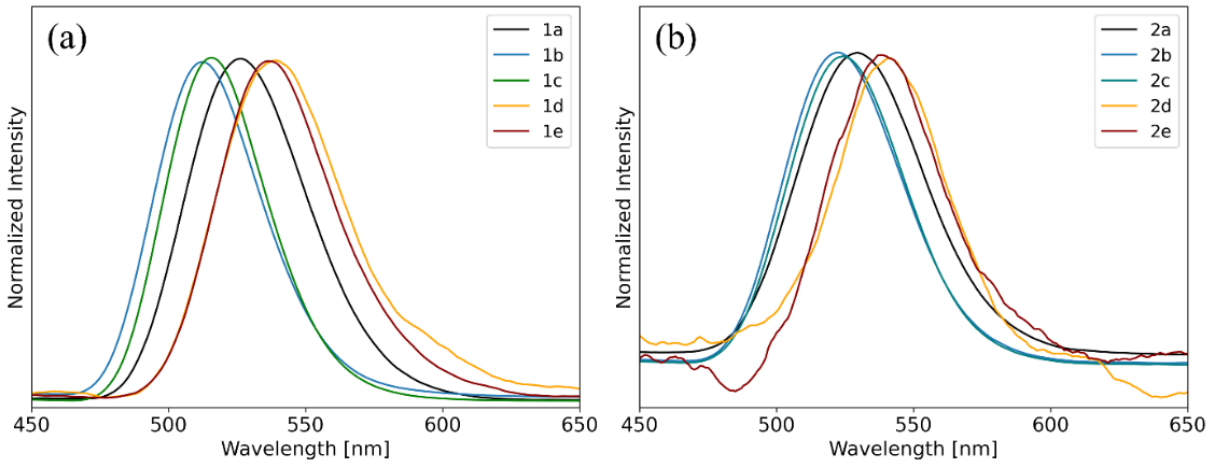

Figure 16. Emission spectra of complexes **1a**–**1e** (a) and **2a**–**2e** (b) at RT.
Noisy baseline of iodine containing samples is due to the low intensity of signals.

Measured emission spectra also provided further insight on the metal-ligand interactions in synthesized halomanganates. As can be seen from the Table 2 and Figure 16, energy of the emission of synthesized halomanganates decreases in the same order for both cations: $[MnBr_4]^{2-} > [MnBr_2Cl_2]^{2-} > [MnCl_4]^{2-} > [MnBr_2I_2]^{2-} > [MnCl_2I_2]^{2-}$. To explain the observed phenomenon, both strength of the ligand fields and nephelauxetic effect of the halogen atoms should be considered. As is known from the spectrochemical series, bromine has a weaker ligand field compared to chlorine, and hence, according to the Tanabe-Sugano diagram displayed in Figure 3, the distance between $^4T_1$ and $^6A_1$ energy levels should be larger, resulting in high-energy emission. This explains why emission maxima of complexes with $[MnBr_4]^{2-}$ anion is slightly blueshifted compared to complexes with $[MnBr_2Cl_2]^{2-}$ anion and even more blueshifted compared to complexes with $[MnCl_4]^{2-}$ anion. On the other hand, iodine has even weaker ligand field, but the emission of complexes with iodine ligands are redshifted compared to other complexes. This can be explained by the fact that iodine has largest nephelauxetic effect among halogens, which means that Mn–I bond has more covalent nature. According to Morad *et al*. [63], this could result in a lower energy of emission in halomanganates with iodine ligands, which is indeed observed. By keeping both arguments in mind, it also possible to explain why complexes with $[MnBr_2I_2]^{2-}$ anion have slightly higher emission energy compared

to $[MnCl_2I_2]^{2-}$, as the emission of former is first redshifted to due nephelauxetic effect of iodine, but then slightly blueshifted due to the ligand field effects of bromine.

The influence of nephelauxetic effect can also be observed from the excitation spectra of synthesized complexes (see Figure 17), as excitation bands of complexes with iodine ligands (**1d**–**1e** and **2d**–**2e**) are noticeably different, indicating a higher degree of mixing between manganese and iodine orbitals. Nevertheless, for all complexes, two distinct groups of excitation bands corresponding to different electronic transitions in manganese(II) center can be observed. By analyzing the electronic transition diagram for Mn(II) ion (see Figure 3, right), it is clear that excitation bands at shorter wavelengths should correspond to the high-energy transitions, *i.e.* $^6A_1 \rightarrow {}^4E(D)$ and $^6A_1 \rightarrow {}^4T_2(D)$, while excitation bands at longer wavelengths should correspond to the low-energy transitions, *i.e.* $^6A_1 \rightarrow {}^4A_1$, $^4E(G)$, $^6A_1 \rightarrow {}^4T_2(G)$ and $^6A_1 \rightarrow {}^4T_1(G)$.

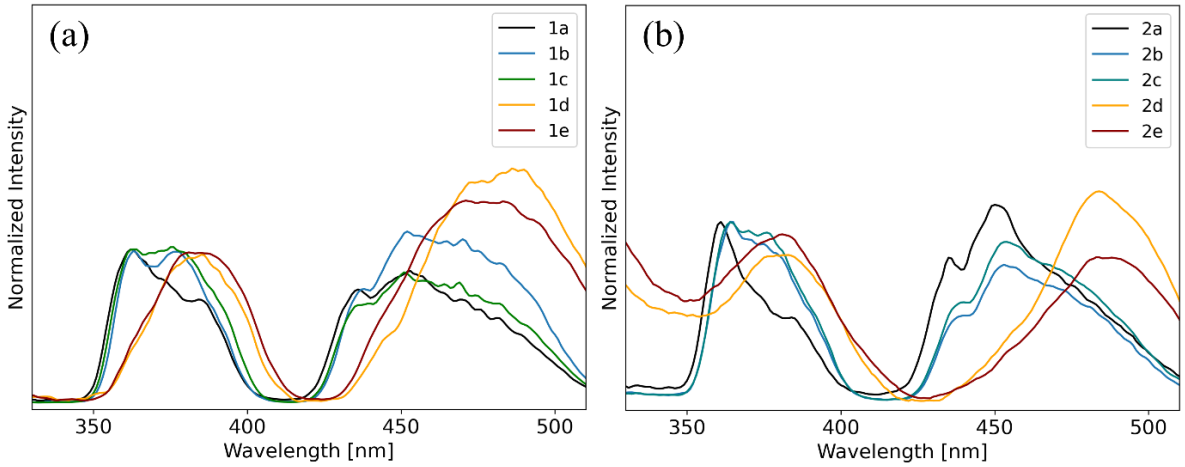

Figure 17. Excitation spectra of complexes **1a**–**1e** (a) and **2a**–**2e** (b) at RT.
Noisy baseline of iodine containing samples is due to the low intensity of signals.

From the excitation spectra, excitation maxima were determined and used in subsequent luminescence emission lifetime and Φ measurements.

3.3.2 Luminescence emission lifetime

Unfortunately, the emission lifetime measurement was not possible for the complexes with iodine ligands due to their low luminescence intensity. For other complexes (**1a**–**1c** and **2a**–**2c**) measurements were conducted without any obstacles; obtained decay curves (Figure 18) were analyzed by using single-exponential and bi-exponential model (Equations 1 and 2).

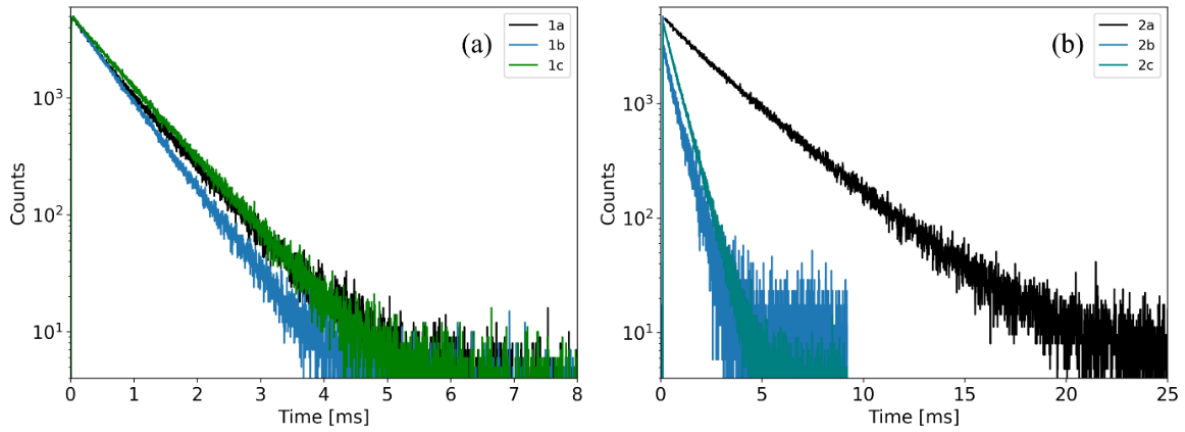

Figure 18. Emission decay curves of complexes **1a**–**1c** (a) and **2a**–**2c** (b) at RT.

As evident from Table 2 and Figure 18, almost all complexes exhibit emission lifetime of about 1 ms, which is in good agreement with previous report on imidazolium-based compounds [79]. Only complex $[BnMIm]_2[MnCl_4]$ (**2a**) had noticeably longer emission lifetime, which was estimated to be almost 3 ms. This underlines the fact that emissive properties of manganese(II) complexes depend not only on the structure of anions, but also on the interaction of anions with counter cations. In case of complex **2a**, most probably, energy levels of excited states of manganese(II) center were the farthest from the energy levels of excited states of 1-benzyl-3-methylimidazolium cation, slowing down the intersystem crossing and increasing the emission lifetime. To prove this theory, in the future energy levels of excited states of halomanganate anions and imidazolium-based cations should be calculated *in silico* and compared with the experimental evidence.

3.3.3 Luminescence quantum yield

Similarly to the emission lifetime measurements, low luminescence intensity of complexes with iodine ligands (**1d**–**1e** and **2d**–**2e**) obstructed the Φ measurements: only for complex **2e** some quantifiable signal could be detected, showing a very poor Φ of 0.01. This result is slightly surprising, since bright luminescence of pyridinium-based mixed-halomanganates with iodine ligands was recently reported by Berezin *et al.* [76]. As mentioned before, complexes with iodine ligands synthesized in current study showed high hygroscopicity, slowly turning into non-luminescent liquids at ambient medium, which may have influenced the Φ measurements. Another argument observed results arises from the intrinsic properties of iodine ligands. It is possible that large nephelauxetic effect of iodine ligands, described above, have increased the energy gap between excited states of manganese(II) center and excited states of imidazolium-based counter cations, thus reducing sensitizing effect of the latter and quenching the

luminescence. In fact, the negative effect of iodine ligands on the luminescence intensity of manganese(II) complexes was reported before [63,80,81], therefore the reason behind exceptional results of Berezin *et al*. remains somewhat unclear. For further understanding of the interaction between iodine ligands and counter cations, more iodine-containing homo- and mixed-halomanganates should be synthesized and analyzed in the future.

Φ measurements of complexes with chlorine and bromine ligands (**1a**–**1c** and **2a**–**2c**) were conducted without any problems. Surprisingly, contrary to the observations made by the naked eye during the experimental section, not the complexes with $[MnBr_2Cl_2]^{2-}$ anion, but the ones with $[MnBr_4]^{2-}$ anion exhibited largest *Φ* values. Let this be a small reminder of the limitations of human vision and that one should always double check the observed results with the according instruments before jumping to the conclusions. Higher *Φ* of complexes of $[MnBr_4]^{2-}$ is most likely promoted by the spin-orbit coupling and the ligand field effects of bromine atoms, which facilitate intersystem crossing between counter cations and manganese(II) centers.

As can be observed from the Table 2, *Φ* values of complexes with $[MnBr_2Cl_2]^{2-}$ anions were in between *Φ* values of complexes with $[MnCl_4]^{2-}$ and $[MnBr_4]^{2-}$ anions. This is also an important result since it demonstrates that *Φ* of halomanganates can be tuned by the halogen composition. Tunable *Φ* is an intriguing property, which may be useful for data encryption and security printing applications [77,78]. As a proof of concept, complexes with the same cations, but different halogen composition (*e.g*. $[MnBrCl_3]^{2-}$ or $[MnBr_3Cl]^{2-}$) should be synthesized and analyzed in the future.

Φ measurement also demonstrated that Mn···Mn distance is not the most crucial factor influencing the intensity of luminescence in Mn(II) complexes: even though complexes with bulkier $[BnMIm]^+$ cation generally exhibited noticeably larger *Φ* values than complexes with $[EMIm]^+$ cation, it was not so for all the complexes. Closer look to the Table 2 reveals that complex **2c** has a smaller *Φ* compare to complex **1c**, while SC-XRD analysis clearly demonstrated that Mn···Mn distance in complex **2c** is larger than in **1c**. Probably, in case of $[MnBr_2Cl_2]^{2-}$ anion, intersystem crossing is more favorable from excited states of $[EMIm]^+$ cation, which, evidently, has more significant impact on *Φ*, than Mn···Mn distance.

Of all complexes, $[BnMIm]_2[MnBr_4]$ (**2b**) had the largest *Φ* of 0.59, a remarkably good result, which fulfilled the aim of current study. As complexes with $[BnMIm]^+$ generally showed superior *Φ* and better crystallinity, it was decided to focus on them during next research stage.

3.3.4 Fabrication of luminescent films

First, similarly to our previous report [94], an attempt to prepare luminescent films by recrystallizing neat complexes **2a**–**2c** on a glass substrates was made. To do so, about ~10 mg of powder samples was fixed between two pieces of glass, which were then held on the hot plate heater set to 150 °C until complete melting. Then, the heating was turned off, and samples were left to crystallize at RT over weekend.

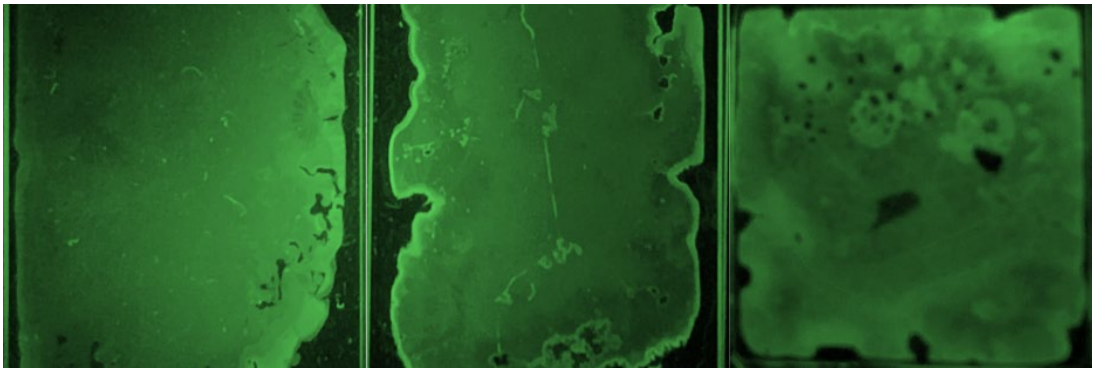

Figure 19. Luminescent films made of **2a** (left), **2b** (middle) and **2c** (right) under UV light.

As depicted in Figure 19, complexes **2a**–**2c** successfully crystallize at ambient conditions, producing thin and luminescent films. This is an important result since it prompts to a simple, solvent-free and energy efficient method to produce emissive layers for OLEDs.

Anionic manganese complexes are known to be sensitive to humidity, with a noticeable decrease in luminescence intensity after absorption of water [26,27]. To protect the complexes **2a**–**2c** from the high humidity of the air, it was decided to dope them into the polymer matrix. It is also important to observe luminescence behavior of complexes in polymer matrix, since in commercial OLED systems light-emitting materials are doped into electron- and hole-transporting materials to achieve higher external quantum efficiency [24]. As a polymer matrix, poly(propylene glycol) terminated with tolylene 2,4-diisocyanate (PPG-TDI) was chosen based on an earlier study by She *et al*. in 2019 [77]. Polymer films were prepared by dispersing PPG-TDI and complexes **2a**–**2c** (10% w/w) in 1 mL of DCM, then transferring the mixture into a Teflon stack and evaporating the solvent at 60 °C for 72 hours. Finally, emission spectra of prepared films were measured to describe luminescence properties of **2a**–**2c** in polymer matrix.

As evident from Figure 20, PPG-TDI matrix resulted in an additional blue light emission band at 400–450 nm. This emission band probably origins from fluorescence of tolylene 2,4-diisocyanate groups inside the polymer. Besides the additional band, polymer matrix had no apparent negative effect on the luminescence properties of complexes **2a**–**2c**: characteristic

emission band at 500-550 nm is still present in all spectra. As expected, polymer film doped with complex **2b** exhibited the brightest luminescence among prepared films.

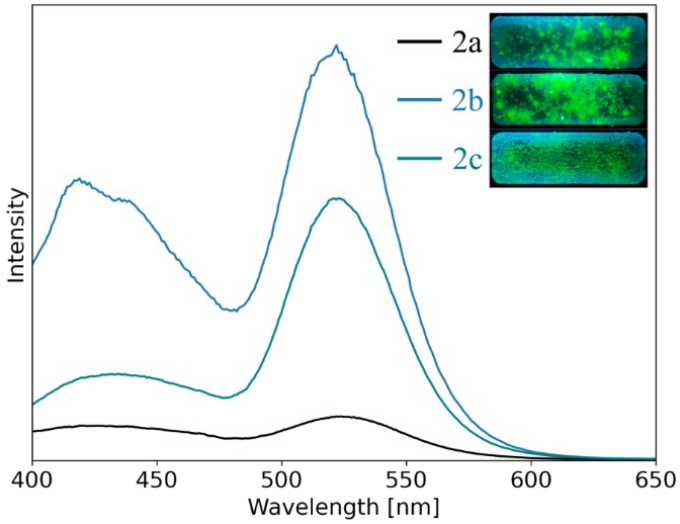

Figure 20. Emission spectra of complexes **2a**–**2c** in polymer matrix.
Inset: photographs of prepared films under UV light.

Good film-forming capability of neat **2a**–**2c**, as well as excellent luminescent properties of polymer films doped with those complexes clearly demonstrate that $[BnMIm]^+$-based halomanganates, especially **2b**, are promising materials to be applied as emitters in new generation OLEDs.

To describe suitability of complex **2b** as an emitter, its optical band gap was estimated next.

3.3.5 Optical band gap

For materials used in light-emitting devices, the optical band gap, *i.e*. the energy gap between highest occupied molecular orbital (HOMO) and lowest unoccupied molecular orbital (LUMO), is a crucial parameter to be considered [95]. A common way to estimate the optical band gap is by determining the absorption onset on the UV-visible absorption spectrum [24], whereas the measurement can be done both in the solution [95] or in the solid state [96]. In case of Mn(II) complexes, optical transitions are spin-forbidden, resulting in relatively low absorption coefficients [63], which makes UV-visible absorption measurements in the solution problematic. Therefore, to estimate optical band gap of complex $[BnMIm]_2[MnBr_4]$ (**2b**), UV-visible absorption measurement was conducted for the powder sample of the complex.

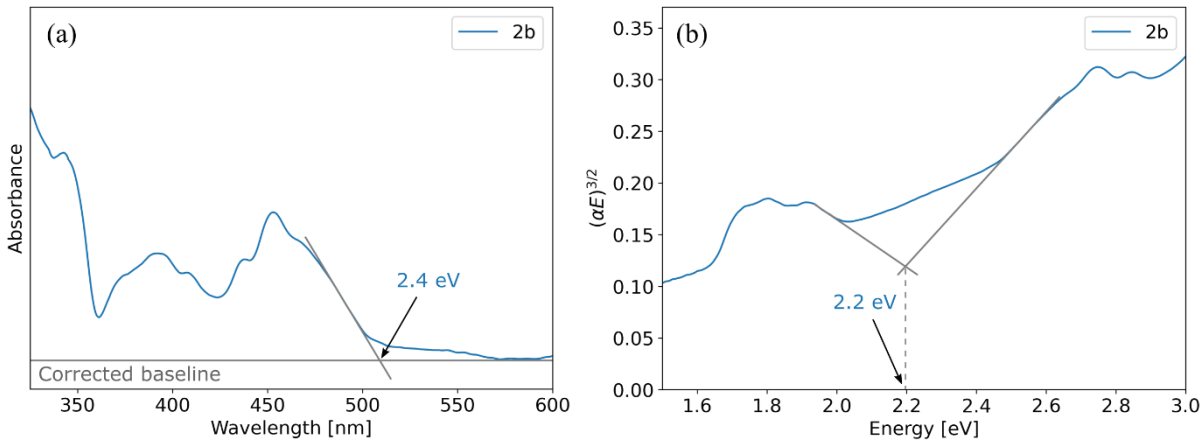

Figure 21. Optical band gap estimation of complex **2b** from the absorption onset (a) and by using Tauc's relation (b).

As detailed in Figure 21 (a), optical band gap of complex **2b** was roughly estimated from the obtained absorption spectra by fitting straight line to the absorption onset and determining its intersection point with the corrected baseline. The intersection was found to be at 509 nm, which corresponds to an optical band gap of approximately 2.4 eV.

Another method to estimate the optical band gap is by using Tauc's relation [95,97], where the optical transition energies (E) calculated from the absorption wavelengths are plotted against quantity $(\alpha E)^{3/2}$; α stands for the measured absorbance. In current study, extrapolation technique suggested by Jubu *et al*. was used to analyze resulting graph [97]. As evident from Figure 21 (b), by using this technique optical band gap of complex **2b** was estimated to be 2.2 eV.

The difference between optical band gap values as shown in Figure 21 is not exceptional [95] and underlines the fact, that both extrapolation techniques are only suitable to provide estimated values. To obtain more precise result, in the future, optical band gap values of complex **2b** obtained from UV-visible absorption spectrum will be compared to the values obtained *in silico* [98] and from the cyclic voltammograms [95], measurements of which are currently in progress.

Estimated optical band gap, as well as the other information, accumulated during current study, will be used to design OLEDs with complex $[BnMIm]_2[MnBr_4]$ (**2b**) applied as an emitter. Fabrication of OLED prototypes is planned in a collaboration with Prof. Tien-Lin Wu laboratory, National Tsing Hua University, Taiwan.

SUMMARY

Current work aimed to prepare highly luminescent anionic manganese(II) complexes. Accordingly, a synthetic procedure was developed and optimized. In total, ten manganese complexes were synthesized, including five complexes with $[EMIm]^+$ cation (**1a**–**1e**) and five complexes with $[BnMIm]^+$ cation (**2a**–**2e**). To the best of our knowledge, eight out of ten synthesized complexes are novel compounds (**1c**–**1e** and **2a**–**2e**). Structures of synthesized complexes were confirmed by nuclear magnetic resonance spectroscopy, elemental analysis, and X-ray diffraction measurements (when possible). All complexes exhibited good thermal stability, which is of great importance for fabrication of optoelectronic devices. Complexes with $[EMIm]^+$ cation were found to be highly liquescent, with the melting points being far below 100 °C, while complexes with $[BnMIm]^+$ cation exhibited higher crystallinity and stability at ambient medium. It was also observed that introduction of iodine ligands resulted in decrease of crystallinity and luminescence intensity of complexes, possibly due to the bulkiness and nephelauxetic effect of iodine ligand.

For all ten anionic complexes, luminescence emission and excitation spectra were measured at room temperature. If the luminescence was bright enough, emission lifetime and quantum yield were also measured. It was observed, that complexes with $[MnBr_4]^{2-}$ anion exhibited brightest luminescence, most probably due to an improved interaction between manganese(II) centers and counter cations. Among prepared complexes, **2b** exhibited largest absolute quantum yield at room temperature (Φ = 0.59). This result fulfilled the initial aim of the current work and prompted a further investigation of the complexes with $[BnMIm]^+$ cation.

Next, it was demonstrated that complexes **2a**–**2c** easily form luminescent crystalline films at ambient conditions and are also suitable to be used as dopants to produce luminescent polymer films. This is important evidence which proves that those complexes can be used as emitters in both non-doped and doped OLEDs.

Finally, optical band gap of complex **2b** was estimated from the onset wavelength of the absorption spectrum and via Tauc's relation.

Based on measurement results, complex **2b** was determined to be the most prominent material to be applied as an emitter in OLED displays. It exhibited remarkable quantum yield at room temperature, short emission lifetime, and it is soluble in commonly used polar solvents, such as water, methanol, or ethanol, which is of high importance for the solution processing. Currently, fabrication of OLED prototypes based on **2b** is in progress.

ACKNOWLEDGMENTS

The author would like to express his deepest appreciation to his supervisors Prof. Hou-Hsiu Chou and Dr. Kaija Põhako-Esko for their support and guidance during the preparation of the current study. The author would also like to thank all members of the Soft Functional Materials & Sustainable Energy Laboratory of National Tsing Hua University, especially Yi-An Chen, for their patience, help and useful advices. Additionally, Pei-Lin Chen and Hui-Chi Tan from the Instrumentation Center of National Tsing Hua University for their help with single crystal X-ray diffraction and Nuclear Magnetic Resonance measurements, and the Elemental Analysis Laboratory of National Chung Hsing University for the elemental analysis measurements. Also, Prof. Masako Kato from Kwansei Gakuin University, for her help with the luminescence quantum yield measurements, as well as Prof. Tien-Lin Wu from National Tsing Hua University and all members of his laboratory, for their interest in the outcomes of current study and their willingness to collaborate.

Finally, the author would like to acknowledge the financial support from Education and Youth Board of Republic of Estonia and University of Tartu Foundation, which greatly contributed to the quality of current study.

KOKKUVÕTE

On raske alahinnata mõju, mida omab ja hakkab omama globaalne soojenemine elu kvaliteedile Maal [1,2]. Selleks, et ära hoida lähenevat katastroofi, on muutused hädavajalikud igal ühiskonnatasandil [3]. Tähtsaimad muutused peavad aga toimuma viisides, kuidas me loome tehnoloogiaid ning tarbime ja taaskasutame materjale.

Üks 21. sajandi silmapaistvamatest tehnoloogilistest innovatsioonidest on orgaanilised valgusdioodid [4]. Tänapäeva ekraanide võtmekomponentidena on orgaanilised valgusdioodid majanduslikult oluline tehnoloogiasuund, mille arengut toetavad suurimad elektroonikaettevõtted nagu LG, Samsung, Sony ja Apple [5–7]. Varsti võivad orgaanilised valgusdioodid mängida veelgi tähtsamat rolli meie argielus: neile ennustatakse kasutust rõivastes ja inimkeha võimalusi laiendavas elektroonilises nahas [8–10].

Vaatamata orgaaniliste valgusdioodide tormilisele eduloole on antud tehnoloogial üks põhimõtteline puudus. Kommertsiaalselt kasutatavad orgaanilised valgusdioodid on taaskasutamiseks kõlbmatud [11,12], mis kõvasti panustab kasvavale elektroonilise prügi probleemile [13,14]. Lisaks kasutatakse siiamaani kommertsiaalsetes orgaanilistes valgusdioodides haruldasi muldmetalle, sealhulgas plaatinat [15,16] ja iriidiumit [17,18]. Seetõttu on tähtis jätkata orgaaniliste valgusdioodide tehnoloogia arendamist, keskendudes just selle jätkusuutlikumaks muutmisele.

Üheks lootustandvaks lahenduseks uue orgaaniliste valgusdioodide põlvkonna jaoks on fosforestsentsetest üleminekumetallide kompleksidest koosnevad valgust kiirgavad materjalid. Näiteks sobivad selleks raud(III) [21], volfram(VI) [22,23] või mangaan(II) [24,25] kompleksid. Hiljuti on eelkõige mangaan(II) kompleksid saanud teadlaste intensiivse tähelepanu osaliseks nende madala tootmishinna, mittetoksilisuse ning muude omaduste tõttu, mille hulgas on näiteks ere fosforestsents, molekulaarse disaini paindlikkus ja kõrge fotofunktsionaalsus [26,27].

Antud töö keskendus taaskasutatavate valgust kiirgavate materjalide arendamisele eesmärgiga rakendada neid orgaanilistes valgusdioodides. Töö on motiveeritud autori isiklikust soovist panustada kliimamuutuste ärahoidmisele ning hiljutistest poliitilistest ja majanduslikest initsiatiividest nagu Euroopa Liidu Rohepööre [28]. Töö peamine eesmärk oli sünteesida valgust kiirgav materjal, mille kvantsaagise väärtus toatemperatuuril oleks vähemalt 0,50.

Molekulaarne disain, mida valiti püstitatud eesmärgi saavutamiseks, keskendus anioonsetest mangaan(II) ühenditest ja imidasooliumkatioonidest koosnevatele kompleksidele. Kokku valmistati kümme kompleksi, kombineerides viite erinevat halomanganaatiooni ja kahte kirjanduse ja katsete põhjal valitud katiooni ([EMIm]$^+$ = 1-etüül-3-metüülimidasooliumioon; [BnMIm]$^+$ = 1-bensüül-3-metüülimidasooliumioon):

- [EMIm]$_2$[MnCl$_4$] (**1a**)
- [EMIm]$_2$[MnBr$_4$] (**1b**)
- [EMIm]$_2$[MnBr$_2$Cl$_2$] (**1c**)
- [EMIm]$_2$[MnCl$_2$I$_2$] (**1d**)
- [EMIm]$_2$[MnBr$_2$I$_2$] (**1e**)
- [BnMIm]$_2$[MnCl$_4$] (**2a**)
- [BnMIm]$_2$[MnBr$_4$] (**2b**)
- [BnMIm]$_2$[MnBr$_2$Cl$_2$] (**2c**)
- [BnMIm]$_2$[MnCl$_2$I$_2$] (**2d**)
- [BnMIm]$_2$[MnBr$_2$I$_2$] (**2e**)

Töö autori teadmiste järgi on kaheksa sünteesitud kompleksidest varem avaldamata (**1c**–**1e** ja **2a**–**2e**). Kõikide komplekside puhtust ja struktuuri kontrolliti tuumamagnetresonants-spektroskoopiaga ning elementanalüüsiga. Kui proovi kvaliteet seda võimaldas, teostati ka pulbri ja/või monokristalli röntgendifraktsioonanalüüsi. Lisaks, uuriti kõikide komplekside sulamis- ja lagunemistemperatuure. Leiti, et [BnMIm]$^+$ katiooniga komplekside sulamistemperatuur on kõrgem võrreldes [EMIm]$^+$ katiooniga kompleksidega, seda tõenäoliselt [BnMIm]$^+$ katiooni aromaatseete rühmade π–π interaktsiooni tõttu. Kõik kompleksid demonstreerisid head termilist stabiilsust, mis on tähtis omadus valgust kiirgavate materjalide puhul, kuna orgaaniliste valgusdioodide valmistamise protsess nõuab tihti kõrgeid temperatuure.

Töö järgmises etapis uuriti sünteesitud komplekside fotofüüsikalisi omadusi. Alguseks mõõdeti kõikide komplekside ergastus- ja emissiooni spektreid tahkes olekus toatemperatuuril. Mõõdetud emissiooni spektreid analüüsides leiti, et sõltumata katioonist väheneb sünteesitud halomanganaatide poolt kiirgava valguse energia järgnevas järjekorras:

$$[MnBr_4]^{2-} > [MnBr_2Cl_2]^{2-} > [MnCl_4]^{2-} > [MnBr_2I_2]^{2-} > [MnCl_2I_2]^{2-}$$

Saadud seaduspära põhjal järeldati, et halomanganaatide kiirgusomadusi määravad nii ligandvälja tugevus kui ka nefelaukseetiline efekt. Joodi aatomite tugeva nefelaukseetilise efekti mõju d–d üleminekutele oli näha ka ergastusspektritel. Järgmisena üritati mõõta sünteesitud komplekside emissiooni eluiga ja kvantsaagist. Leiti, et joodi sisaldavate komplekside (**1d**, **1e**, **2d** ja **2e**) emissiooni intensiivsus on liiga nõrk usaldusväärsete emissiooni eluea või kvantsaagiste määramiseks. Kompleksite **1a**–**1c** ja **2a**–**2c** puhul mõõtmised

õnnestusid. Mõõtmiste tulemused näitasid, et nii emissiooni eluiga kui ka kvantsaagis sõltuvad tugevalt aniooni ligandide olemusest. Mida rohkem on halomanganaatioonis broomi aatomeid, seda lühem on vastavate komplekside emissiooni eluiga ja seda suurem on nende kvantsaagise väärtus. See tulemus on heas kooskõlas kvantmehaanikast tuletatud teooriaga, mis ennustab, et raskemad aatomid peaksid suurendama spinn-orbitaalset põimumist ning selle kaudu kiirendama fosforestsentsi. Teatud mõju kvantsaagisele oli ka katioonil - üldiselt oli $[BnMIm]^+$ katiooniga kompleksidel suurem kvantsaagis. Kõikide valmistatud ühendite seast suurim kvantsaagis oli kompleksil $[BnMIm]_2[MnBr_4]$ (**2b**): $\Phi = 0.59$. See väärtus saavutas käesoleva töö eesmärgi ning inspireeris edasist uurimustööd $[BnMIm]^+$ katiooniga komplekside alal.

Järgmises töö etapis demonstreeriti komplekside **2a**–**2c** kasutamist valgust kiirgavate materjalidena kahes orgaanilistes valgusdioodides levinud vormis: puhta tahke kilena ja lisatuna polümeersesse maatriksisse. Kõigist kolmest kompleksist õnnestus valmistada luminestsentne kile ümbersulatamise teel. See omadus peaks võimaldama nende ühendite otsest kasutamist valgust kiirgava kihina vältides valmistamisprotsessis keskkonnale kahjulike solventide kasutamist või energeetiliselt kulukat vaakumsadestamist. Kompleksid **2a**–**2c** ei kaotanud iseloomulikku fosforestsentsi ka polümeerses maatriksis. See on tähtis omadus, sest see võimaldab nende kasutamist segakoostisega valgust kiirgavates kihtides, mis üldjuhul juhivad eksitone paremini.

Töö viimane etapp keskendus kompleksi **2b** optilise keelutsooni määramisele. Optiline keelutsoon on üks olulisematest parameetritest orgaaniliste valgusdioodide disainimisel, kuna see määrab, milliseid materjale tuleb kasutada elektrone ja auke juhtivate kihtidena. Usaldusväärsema tulemuse saamiseks hinnati kompleksi **2b** optilist keelutsooni kahel erineval viisil: otse absoprtsioonispektrist ja Tauc'i graafikut konstrueerides.

Käesoleva töö jooksul valmistati ja uuriti kümmet anioonset mangaan(II) kompleksi. Sünteesitud kompleksite seast on kompleks $[BnMIm]_2[MnBr_4]$ (**2b**) kahtlemata perspektiivseim materjal orgaanilistes valgusdioodides kasutamiseks selle märkimisväärse kvantsaagise, lühikese emissiooni eluea ja energeetiliselt sobiliku optilise keelutsooni tõttu. Kompleksist **2b** on lihtne valmistada läbipaistvaid valgust kiirgavaid kilesid ning selle luminestsentsed omadused ei kao ka polümeerses maatriksis. Kompleksil **2b** põhinevate orgaaniliste valgusdioodide prototüübid on hetkel testimisel partnerlaboris, Tsing Hua Rahvusülikoolis, Taiwanis.

REFERENCES

[1] K. Abbass, M.Z. Qasim, H. Song, M. Murshed, H. Mahmood, I. Younis, A review of the global climate change impacts, adaptation, and sustainable mitigation measures, Environ. Sci. Pollut. Res. 29 (2022) 42539–42559.

[2] S.G. Yalew, M.T.H. van Vliet, D.E.H.J. Gernaat, F. Ludwig, A. Miara, C. Park, et al., Impacts of climate change on energy systems in global and regional scenarios, Nat. Energy. 5 (2020) 794–802.

[3] P. Bauer, B. Stevens, W. Hazeleger, A digital twin of Earth for the green transition, Nat. Clim. Change. 11 (2021) 80–83.

[4] G. Hong, X. Gan, C. Leonhardt, Z. Zhang, J. Seibert, J.M. Busch, et al., A Brief History of OLEDs—Emitter Development and Industry Milestones, Adv. Mater. 33 (2021) 2005630.

[5] Y. Huang, E.-L. Hsiang, M.-Y. Deng, S.-T. Wu, Mini-LED, Micro-LED and OLED displays: present status and future perspectives, Light Sci. Appl. 9 (2020) 105.

[6] H.-W. Chen, J.-H. Lee, B.-Y. Lin, S. Chen, S.-T. Wu, Liquid crystal display and organic light-emitting diode display: present status and future perspectives, Light Sci. Appl. 7 (2018) 17168–17168.

[7] D. Corrêa Santos, M. de F. Vieira Marques, Blue light polymeric emitters for the development of OLED devices, J. Mater. Sci. Mater. Electron. 33 (2022) 12529–12565.

[8] T. Someya, Z. Bao, G.G. Malliaras, The rise of plastic bioelectronics, Nature. 540 (2016) 379–385.

[9] M.S. White, M. Kaltenbrunner, E.D. Głowacki, K. Gutnichenko, G. Kettlgruber, I. Graz, et al., Ultrathin, highly flexible and stretchable PLEDs, Nat. Photonics. 7 (2013) 811–816.

[10] M. Vosgueritchian, J.B.-H. Tok, Z. Bao, Light-emitting electronic skin, Nat. Photonics. 7 (2013) 769–771.

[11] I.B. Kang, C.W. Han, J.K. Jeong (Eds.), Advanced Display Technology: Next Generation Self-Emitting Displays, Springer Singapore, Singapore, 2021.

[12] D. Volz, M. Wallesch, C. Fléchon, M. Danz, A. Verma, J.M. Navarro, et al., From iridium and platinum to copper and carbon: new avenues for more sustainability in organic light-emitting diodes, Green Chem. 17 (2015) 1988–2011.

[13] R. Rautela, S. Arya, S. Vishwakarma, J. Lee, K.-H. Kim, S. Kumar, E-waste management and its effects on the environment and human health, Sci. Total Environ. 773 (2021) 145623.

[14] J.-M. Yeom, H.-J. Jung, S.-Y. Choi, D.S. Lee, S.-R. Lim, Environmental Effects of the Technology Transition from Liquid–Crystal Display (LCD) to Organic Light-Emitting Diode (OLED) Display from an E-Waste Management Perspective, Int. J. Environ. Res. 12 (2018) 479–488.

[15] J.R. Brandt, X. Wang, Y. Yang, A.J. Campbell, M.J. Fuchter, Circularly Polarized Phosphorescent Electroluminescence with a High Dissymmetry Factor from PHOLEDs Based on a Platinahelicene, J. Am. Chem. Soc. 138 (2016) 9743–9746.

[16] W.C.H. Choy, W.K. Chan, Y. Yuan, Recent Advances in Transition Metal Complexes and Light-Management Engineering in Organic Optoelectronic Devices, Adv. Mater. 26 (2014) 5368–5399.

[17] A.K. Pal, S. Krotkus, M. Fontani, C.F.R. Mackenzie, D.B. Cordes, A.M.Z. Slawin, et al., High-Efficiency Deep-Blue-Emitting Organic Light-Emitting Diodes Based on Iridium(III) Carbene Complexes, Adv. Mater. 30 (2018) 1804231.

[18] D. Ma, T. Tsuboi, Y. Qiu, L. Duan, Recent Progress in Ionic Iridium(III) Complexes for Organic Electronic Devices, Adv. Mater. 29 (2017) 1603253.

[19] C. Adachi, Third-generation organic electroluminescence materials, Jpn. J. Appl. Phys. 53 (2014) 060101.

[20] H. Uoyama, K. Goushi, K. Shizu, H. Nomura, C. Adachi, Highly efficient organic light-emitting diodes from delayed fluorescence, Nature. 492 (2012) 234–238.

[21] P. Chábera, Y. Liu, O. Prakash, E. Thyrhaug, A.E. Nahhas, A. Honarfar, et al., A low-spin Fe(III) complex with 100-ps ligand-to-metal charge transfer photoluminescence, Nature. 543 (2017) 695–699.

[22] K.-T. Yeung, W.-P. To, C. Sun, G. Cheng, C. Ma, G.S.M. Tong, et al., Luminescent Tungsten(VI) Complexes: Photophysics and Applicability to Organic Light-Emitting Diodes and Photocatalysis, Angew. Chem. Int. Ed. 56 (2017) 133–137.

[23] K.-T. Chan, T.-L. Lam, D. Yu, L. Du, D.L. Phillips, C.-L. Kwong, et al., Strongly Luminescent Tungsten Emitters with Emission Quantum Yields of up to 84 %: TADF and High-Efficiency Molecular Tungsten OLEDs, Angew. Chem. Int. Ed. 58 (2019) 14896–14900.

[24] L.-J. Xu, C.-Z. Sun, H. Xiao, Y. Wu, Z.-N. Chen, Green-Light-Emitting Diodes based on Tetrabromide Manganese(II) Complex through Solution Process, Adv. Mater. 29 (2017) 1605739.

[25] Y. Qin, P. Tao, L. Gao, P. She, S. Liu, X. Li, et al., Designing Highly Efficient Phosphorescent Neutral Tetrahedral Manganese(II) Complexes for Organic Light-Emitting Diodes, Adv. Opt. Mater. 7 (2019) 1801160.

[26] P. Tao, S.-J. Liu, W.-Y. Wong, Phosphorescent Manganese(II) Complexes and Their Emerging Applications, Adv. Opt. Mater. 8 (2020) 2000985.

[27] Y. Qin, P. She, X. Huang, W. Huang, Q. Zhao, Luminescent manganese(II) complexes: Synthesis, properties and optoelectronic applications, Coord. Chem. Rev. 416 (2020) 213331.

[28] E. Bova, Green Budgeting Practices in the EU: A First Review, Directorate General Economic and Financial Affairs (DG ECFIN), European Commission, 2021.

[29] B. Valeur, M.N. Berberan-Santos, A Brief History of Fluorescence and Phosphorescence before the Emergence of Quantum Theory, J. Chem. Educ. 88 (2011) 731–738.

[30] P.B. O'Hara, W. St. Peter, C. Engelson, Turning on the Light: Lessons from Luminescence, J. Chem. Educ. 82 (2005) 49.

[31] C. Ronda (Eds.), Luminescence: From Theory to Applications, John Wiley & Sons, Weinheim, 2007.

[32] M.Y. Berezin, S. Achilefu, Fluorescence Lifetime Measurements and Biological Imaging, Chem. Rev. 110 (2010) 2641–2684.

[33] S.W.S. McKeever, R. Chen, Luminescence models, Radiat. Meas. 27 (1997) 625–661.

[34] J.-R. Albani, Structure and Dynamics of Macromolecules: Absorption and Fluorescence Studies, Elsevier Science, Amsterdam, 2004.

[35] J.R. Lakowicz (Eds.), Instrumentation for Fluorescence Spectroscopy, in: Princ. Fluoresc. Spectrosc., Springer US, Boston, 2006, p. 27–61.

[36] J.R. Lakowicz, ed., Introduction to Fluorescence, in: Princ. Fluoresc. Spectrosc., Springer US, Boston, 2006, p. 1–26.

[37] C. Würth, D. Geißler, T. Behnke, M. Kaiser, U. Resch-Genger, Critical review of the determination of photoluminescence quantum yields of luminescent reporters, Anal. Bioanal. Chem. 407 (2015) 59–78.

[38] C. Würth, J. Pauli, C. Lochmann, M. Spieles, U. Resch-Genger, Integrating Sphere Setup for the Traceable Measurement of Absolute Photoluminescence Quantum Yields in the Near Infrared, Anal. Chem. 84 (2012) 1345–1352.

[39] S.A. VanSlyke, C.W. Tang, L.C. Roberts, Electroluminescent device with organic luminescent medium, US4720432A, 1988.

[40] C.W. Tang, S.A. VanSlyke, C.H. Chen, Electroluminescence of doped organic thin films, J. Appl. Phys. 65 (1989) 3610–3616.

[41] C. Adachi, T. Tsutsui, S. Saito, Blue light-emitting organic electroluminescent devices, Appl. Phys. Lett. 56 (1990) 799–801.

[42] M.A. Baldo, D.F. O'Brien, Y. You, A. Shoustikov, S. Sibley, M.E. Thompson, et al., Highly efficient phosphorescent emission from organic electroluminescent devices, Nature. 395 (1998) 151–154.

[43] K. Dedeian, P.I. Djurovich, F.O. Garces, G. Carlson, R.J. Watts, A new synthetic route to the preparation of a series of strong photoreducing agents: fac-tris-ortho-metalated complexes of iridium(III) with substituted 2-phenylpyridines, Inorg. Chem. 30 (1991) 1685–1687.

[44] T. Huang, W. Jiang, L. Duan, Recent progress in solution processable TADF materials for organic light-emitting diodes, J. Mater. Chem. C. 6 (2018) 5577–5596.

[45] M. Godumala, S. Choi, M.J. Cho, D.H. Choi, Thermally activated delayed fluorescence blue dopants and hosts: from the design strategy to organic light-emitting diode applications, J. Mater. Chem. C. 4 (2016) 11355–11381.

[46] S.K. Jeon, H.L. Lee, K.S. Yook, J.Y. Lee, Recent Progress of the Lifetime of Organic Light-Emitting Diodes Based on Thermally Activated Delayed Fluorescent Material, Adv. Mater. 31 (2019) 1803524.

[47] J.-M. Teng, Y.-F. Wang, C.-F. Chen, Recent progress of narrowband TADF emitters and their applications in OLEDs, J. Mater. Chem. C. 8 (2020) 11340–11353.

[48] J. Han, Z. Huang, X. Lv, J. Miao, Y. Qiu, X. Cao, et al., Simple Molecular Design Strategy for Multiresonance Induced TADF Emitter: Highly Efficient Deep Blue to Blue Electroluminescence with High Color Purity, Adv. Opt. Mater. 10 (2022) 2102092.

[49] V.N. Hamanaka, E. Salsberg, F.J. Fonseca, H. Aziz, Investigating the influence of the solution-processing method on the morphological properties of organic semiconductor films and their impact on OLED performance and lifetime, Org. Elect. 78 (2020) 105509.

[50] X. Yin, Y. He, X. Wang, Z. Wu, E. Pang, J. Xu, et al., Recent Advances in Thermally Activated Delayed Fluorescent Polymer—Molecular Designing Strategies, Front. Chem. 8 (2020) 725.

[51] J.-H. Kim, J.-W. Park, Intrinsically stretchable organic light-emitting diodes, Sci. Adv. 7 (2021) 9715.

[52] S.H. Han, J.Y. Lee, Spatial separation of sensitizer and fluorescent emitter for high quantum efficiency in hyperfluorescent organic light-emitting diodes, J. Mater. Chem. C. 6 (2018) 1504–1508.

[53] S.K. Jeon, H.-J. Park, J.Y. Lee, Highly Efficient Soluble Blue Delayed Fluorescent and Hyperfluorescent Organic Light-Emitting Diodes by Host Engineering, ACS Appl. Mater. Interfaces. 10 (2018) 5700–5705.

[54] J. Adachi, H. Kakizoe, P.K.D. Tsang, A. Endo, 10.1: Invited Paper: Hyperfluorescence™; a Game Changing Technology of OLED Display, SID Symp. Dig. Tech. Pap. 50 (2019) 95–98.

[55] X.-L. Chen, C.-S. Lin, X.-Y. Wu, R. Yu, T. Teng, Q.-K. Zhang, et al., Highly efficient cuprous complexes with thermally activated delayed fluorescence and simplified solution process OLEDs using the ligand as host, J. Mater. Chem. C. 3 (2015) 1187–1195.

[56] M. Wallesch, A. Verma, C. Fléchon, H. Flügge, D.M. Zink, S.M. Seifermann, et al., Towards Printed Organic Light-Emitting Devices: A Solution-Stable, Highly Soluble CuI–NHetPHOS, Chem. – Eur. J. 22 (2016) 16400–16405.

[57] A. Verma, D.M. Zink, C. Fléchon, J. Leganés Carballo, H. Flügge, J.M. Navarro, et al., Efficient, inkjet-printed TADF-OLEDs with an ultra-soluble NHetPHOS complex, Appl. Phys. A. 122 (2016) 191.

[58] J.M. Busch, D.M. Zink, P.D. Martino-Fumo, F.R. Rehak, P. Boden, S. Steiger, et al., Highly soluble fluorine containing Cu(I) AlkylPyrPhos TADF complexes, Dalton Trans. 48 (2019) 15687–15698.

[59] F.Albert. Cotton, D.M.L. Goodgame, Margaret. Goodgame, Absorption Spectra and Electronic Structures of Some Tetrahedral Manganese(II) Complexes, J. Am. Chem. Soc. 84 (1962) 167–172.

[60] H.G.M. Edwards, M.J. Ware, L.A. Woodward, Vibrational spectra and stretching force-constants of tetrahalogeno-complexes of manganese(II), Chem. Commun. Lond. (1968) 540–541.

[61] M. Wrighton, D. Ginley, Excited state decay of tetrahalomanganese(ii) complexes, Chem. Phys. 4 (1974) 295–299.

[62] G.E. Hardy, J.I. Zink, Triboluminescence and pressure dependence of the photoluminescence of tetrahedral manganese(II) complexes, In. Ch. 15 (1976) 3061–3065.

[63] V. Morad, I. Cherniukh, L. Pöttschacher, Y. Shynkarenko, S. Yakunin, M.V. Kovalenko, Manganese(II) in Tetrahedral Halide Environment: Factors Governing Bright Green Luminescence, Chem. Mater. 31 (2019) 10161–10169.

[64] Y.-L. Wei, J. Jing, C. Shi, H.-Y. Ye, Z.-X. Wang, Y. Zhang, High quantum yield and unusual photoluminescence behaviour in tetrahedral manganese(II) based on hybrid compounds, Inorg. Chem. Front. 5 (2018) 2615–2619.

[65] T. Peppel, M. Geppert-Rybczyńska, C. Neise, U. Kragl, M. Köckerling, Low-Melting Manganese(II)-Based Ionic Liquids: Syntheses, Structures, Properties and Influence of Trace Impurities, Materials. 12 (2019) 3764.

[66] M.-E. Sun, Y. Li, X.-Y. Dong, S.-Q. Zang, Thermoinduced structural-transformation and thermochromic luminescence in organic manganese chloride crystals, Chem. Sci. 10 (2019) 3836–3839.

[67] L. Xu, A. Plaviak, X. Lin, M. Worku, Q. He, M. Chaaban, et al., Metal Halide Regulated Photophysical Tuning of Zero-Dimensional Organic Metal Halide Hybrids: From Efficient Phosphorescence to Ultralong Afterglow, Angew. Chem. Int. Ed. 59 (2020) 23067–23071.

[68] Y. Zhang, D. Chen, K.-H. Jin, S.-Q. Zang, Q.-L. Wang, Room-temperature phosphorescence of manganese-based metal halides, Dalt. Trans. 50 (2021) 17275–17280.

[69] C. Jiang, Q. Luo, C. Luo, H. Lin, H. Peng, Thermoinduced structural-transformation and luminescent conversion in hybrid manganese halides, J. Phys. Condens. Matter. 34 (2022) 154001.

[70] X.-W. Cai, Y.-Y. Zhao, H. Li, C.-P. Huang, Z. Zhou, Lead-free/rare earth-free Green-light-emitting crystal based on organic-inorganic hybrid [(C10H16N)2][MnBr4] with high emissive quantum yields and large crystal size, J. Mol. Struct. 1161 (2018) 262–266.

[71] L.-K. Gong, Q.-Q. Hu, F.-Q. Huang, Z.-Z. Zhang, N.-N. Shen, B. Hu, et al., Efficient modulation of photoluminescence by hydrogen bonding interactions between inorganic [MnBr4]2− anions and organic cations, Chem. Commun. 55 (2019) 7303–7306.

[72] G. Zhou, Z. Liu, J. Huang, M.S. Molokeev, Z. Xiao, C. Ma, et al., Unraveling the Near-Unity Narrow-Band Green Emission in Zero-Dimensional Mn2+-Based Metal Halides: A Case Study of (C10H16N)2Zn1–xMnxBr4 Solid Solutions, J. Phys. Chem. Lett. 11 (2020) 5956–5962.

[73] G. Hu, B. Xu, A. Wang, Y. Guo, J. Wu, F. Muhammad, et al., Stable and Bright Pyridine Manganese Halides for Efficient White Light-Emitting Diodes, Adv. Funct. Mater. 31 (2021) 2011191.

[74] G. Zhou, J. Ding, X. Jiang, J. Zhang, M. S. Molokeev, Q. Ren, et al., Coordination units of Mn 2+ modulation toward tunable emission in zero-dimensional bromides for white light-emitting diodes, J. Mater. Chem. C. 10 (2022) 2095–2102.

[75] C. Jiang, H. Fu, Y. Han, D. Li, H. Lin, B. Li, et al., Tuning the Crystal Structure and Luminescence of Pyrrolidinium Manganese Halides via Halide Ions, Cryst. Res. Technol. 54 (2019) 1800236.

[76] A.S. Berezin, M.P. Davydova, D.G. Samsonenko, T.S. Sukhikh, A.V. Artem'ev, A family of brightly emissive homo- and mixed-halomanganates(II): The effect of halide on optical and magnetic properties, J. Lumin. 236 (2021) 118069.

[77] P. She, Y. Ma, Y. Qin, M. Xie, F. Li, S. Liu, et al., Dynamic Luminescence Manipulation for Rewritable and Multi-level Security Printing, Matter. 1 (2019) 1644–1655.

[78] Z. Huang, M. Yi, Y. Xu, P. Qi, Y. Liu, A. Song, et al., Fluorescent magnetic ionic liquids with multiple responses to temperature, humidity and organic vapors, J. Mater. Chem. C. 9 (2021) 13276–13285.

[79] S. Pitula, A.-V. Mudring, Synthesis, Structure, and Physico-optical Properties of Manganate(II)-Based Ionic Liquids, Chem. – Eur. J. 16 (2010) 3355–3365.

[80] J. Chen, Q. Zhang, F.-K. Zheng, Z.-F. Liu, S.-H. Wang, A.-Q. Wu, et al., Intense photo- and tribo-luminescence of three tetrahedral manganese(II) dihalides with chelating bidentate phosphine oxide ligand, Dalton Trans. 44 (2015) 3289–3294.

[81] M. Bortoluzzi, J. Castro, F. Enrichi, A. Vomiero, M. Busato, W. Huang, Green-emitting manganese (II) complexes with phosphoramide and phenylphosphonic diamide ligands, Inorg. Chem. Commun. 92 (2018) 145–150.

[82] L. Mao, P. Guo, S. Wang, A.K. Cheetham, R. Seshadri, Design Principles for Enhancing Photoluminescence Quantum Yield in Hybrid Manganese Bromides, J. Am. Chem. Soc. 142 (2020) 13582–13589.

[83] H.-M. Pan, Q.-L. Yang, X.-X. Xing, J.-P. Li, F.-L. Meng, X. Zhang, et al., Enhancement of the photoluminescence efficiency of hybrid manganese halides through rational structural design, Chem. Commun. 57 (2021) 6907–6910.

[84] L.J. Bourhis, O.V. Dolomanov, R.J. Gildea, J.A.K. Howard, H. Puschmann, The anatomy of a comprehensive constrained, restrained refinement program for the modern computing environment - Olex2 dissected, Acta Crystallogr. Sect. Found. Adv. 71 (2015) 59–75.

[85] G.M. Sheldrick, SHELXT – Integrated space-group and crystal-structure determination, Acta Crystallogr. Sect. Found. Adv. 71 (2015) 3–8.

[86] O.V. Dolomanov, L.J. Bourhis, R.J. Gildea, J. a. K. Howard, H. Puschmann, OLEX2: a complete structure solution, refinement and analysis program, J. Appl. Crystallogr. 42 (2009) 339–341.

[87] G.M. Sheldrick, Crystal structure refinement with SHELXL, Acta Crystallogr. Sect. C Struct. Chem. 71 (2015) 3–8.

[88] C.F. Macrae, I. Sovago, S.J. Cottrell, P.T.A. Galek, P. McCabe, E. Pidcock, et al., Mercury 4.0: from visualization to analysis, design and prediction, J. Appl. Crystallogr. 53 (2020) 226–235.

[89] N.S. Gill, F.B. Taylor, W.E. Hatfield, W.E. Parker, C.S. Fountain, F.L. Bunger, Tetrahalo Complexes of Dipositive Metals in the First Transition Series, in: Inorg. Synth., John Wiley & Sons, Weinheim, 1967, p. 136–142.

[90] H. Shirota, H. Matsuzaki, S. Ramati, J.F. Wishart, Effects of Aromaticity in Cations and Their Functional Groups on the Low-Frequency Spectra and Physical Properties of Ionic Liquids, J. Phys. Chem. B. 119 (2015) 9173–9187.

[91] F. Yao, J. Peng, R. Li, W. Li, P. Gui, B. Li, et al., Room-temperature liquid diffused separation induced crystallization for high-quality perovskite single crystals, Nat. Commun. 11 (2020) 1194.

[92] W.R. Dawson, M.W. Windsor, Fluorescence yields of aromatic compounds, J. Phys. Chem. 72 (1968) 3251–3260.

[93] M.J. Earle, K.R. Seddon, Light emitting complex salts, WO2006043110A1, 2006.

[94] M. Yoshida, V. Sääsk, D. Saito, N. Yoshimura, J. Takayama, S. Hiura, et al., Thermo- and Mechano-Triggered Luminescence ON/OFF Switching by Supercooled Liquid/Crystal Transition of Platinum(II) Complex Thin Films, Adv. Opt. Mater. 10 (2022) 2102614.

[95] M.-M. Duvenhage, M. Ntwaeaborwa, H.G. Visser, P.J. Swarts, J.C. Swarts, H.C. Swart, Determination of the optical band gap of Alq3 and its derivatives for the use in two-layer OLEDs, Opt. Mater. 42 (2015) 193–198.

[96] R. Schlaf, P.G. Schroeder, M.W. Nelson, B.A. Parkinson, C.D. Merritt, L.A. Crisafulli, et al., Determination of interface dipole and band bending at the Ag/tris (8-hydroxyquinolinato) gallium organic Schottky contact by ultraviolet photoemission spectroscopy, Surf. Sci. 450 (2000) 142–152.

[97] P.R. Jubu, F.K. Yam, V.M. Igba, K.P. Beh, Tauc-plot scale and extrapolation effect on bandgap estimation from UV–vis–NIR data – A case study of β-Ga2O3, J. Solid State Chem. 290 (2020) 121576.

[98] S.X. Tao, X. Cao, P.A. Bobbert, Accurate and efficient band gap predictions of metal halide perovskites using the DFT-1/2 method: GW accuracy with DFT expense, Sci. Rep. 7 (2017) 14386.

APPENDICES

Appendix 1. Reagents and solvents used.

Benzoyl chloride (99% purity), chlorocyclohexane (99% purity), manganese(II) chloride (99% purity), manganese(II) bromide tetrahydrate (98% purity), [EMIm]Cl (99% purity), [EMIm]Br (98% purity) and [EMIm]I (99% purity) were purchased from Nova Materials Co., Ltd.

Benzyl chloride (99% purity), benzyl bromide (99% purity), 1-methylimidazole (99% purity), manganese(II) iodide anhydrous (98% purity) and sodium iodide (99+% purity) were purchased from Alfa Aesar.

Acetonitrile (HPLC grade), methanol (BakerDRY™), diethyl ether (A.C.S Reagent) and acetone (N.F.) were purchased from Avantor Performance Materials, Inc.

Appendix 2. Structures of complexes **1a**–**1e** and **2a**–**2e**.

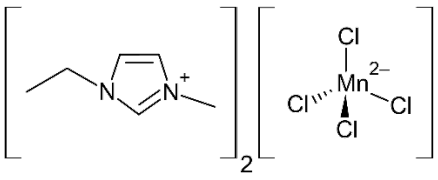

1a

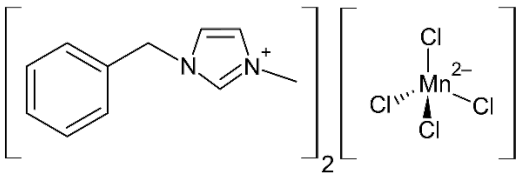

2a

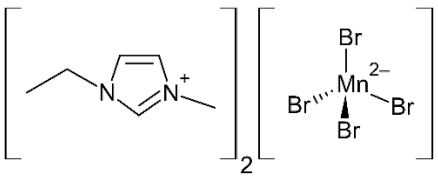

1b

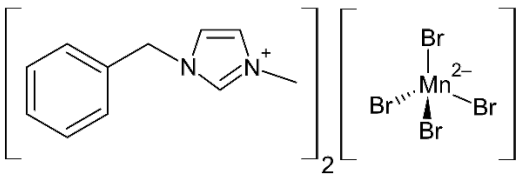

2b

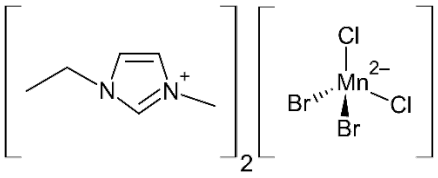

1c

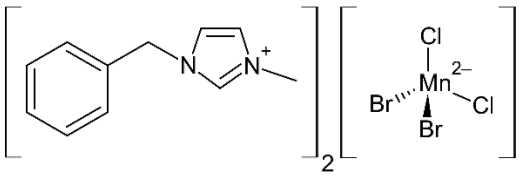

2c

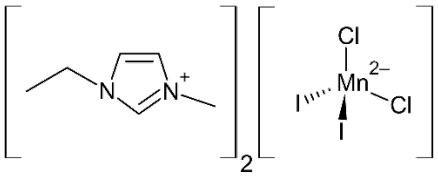

1d

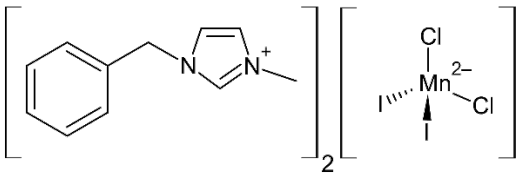

2d

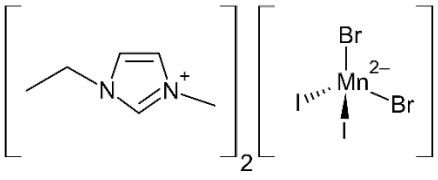

1e

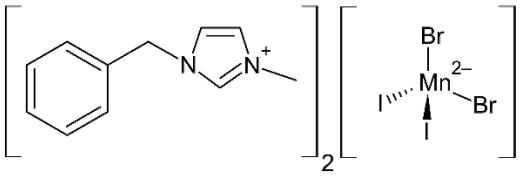

2e

Appendix 3. Selected ^{1}H NMR spectra of synthesized compounds.

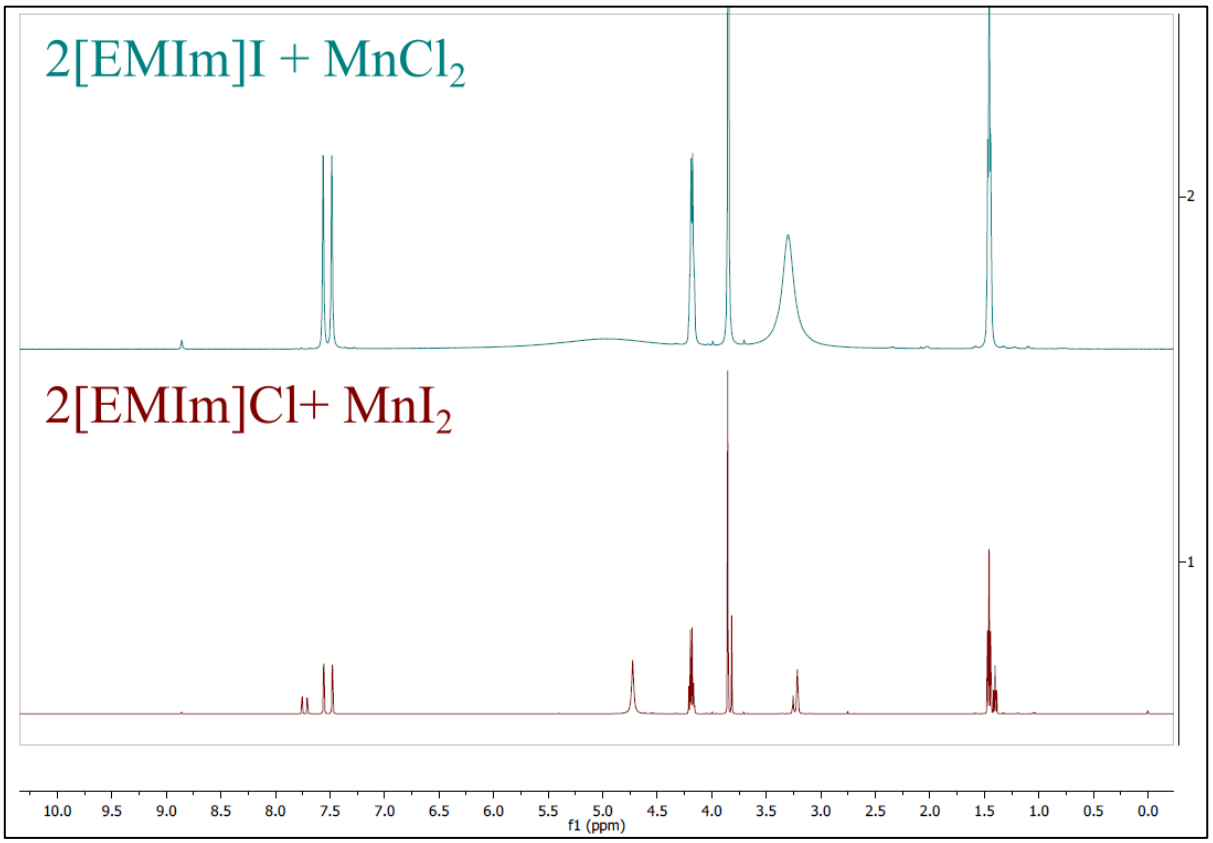

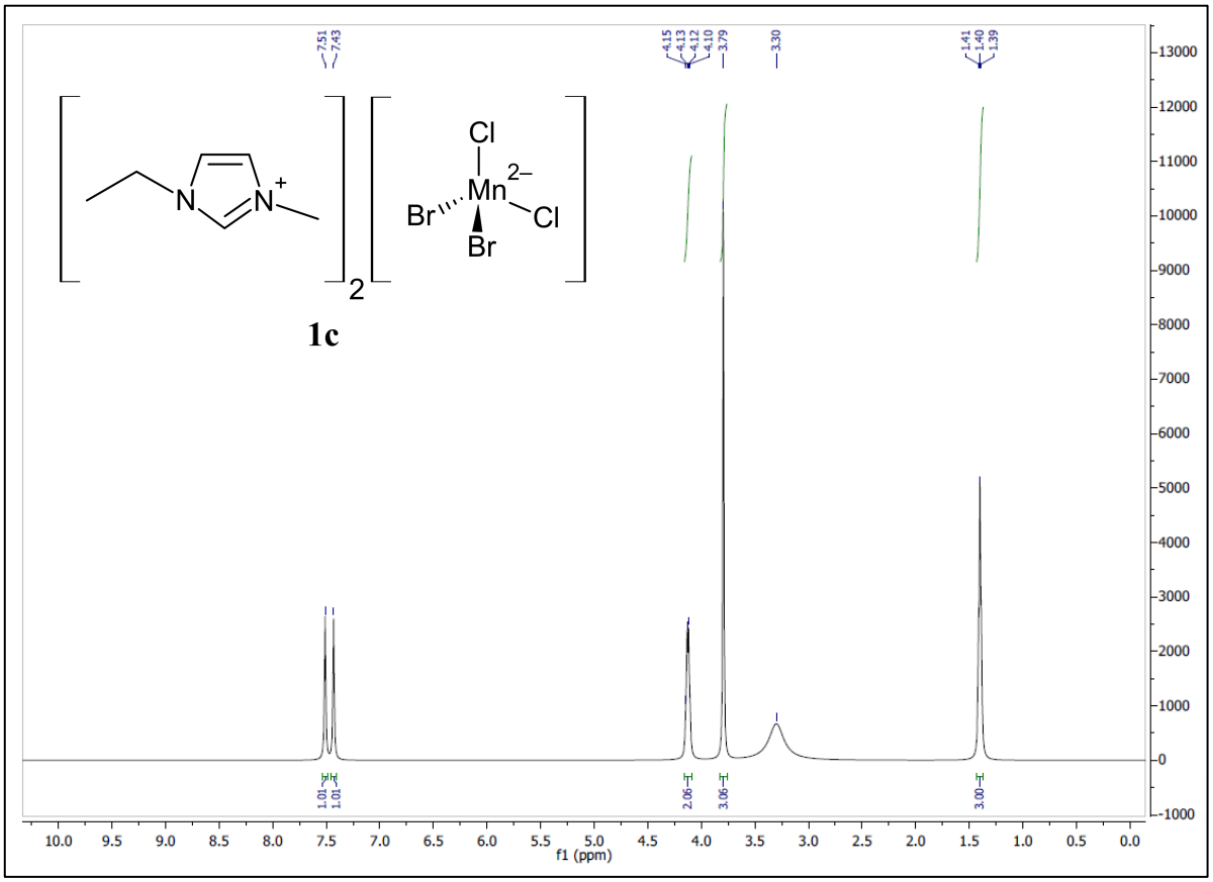

1c

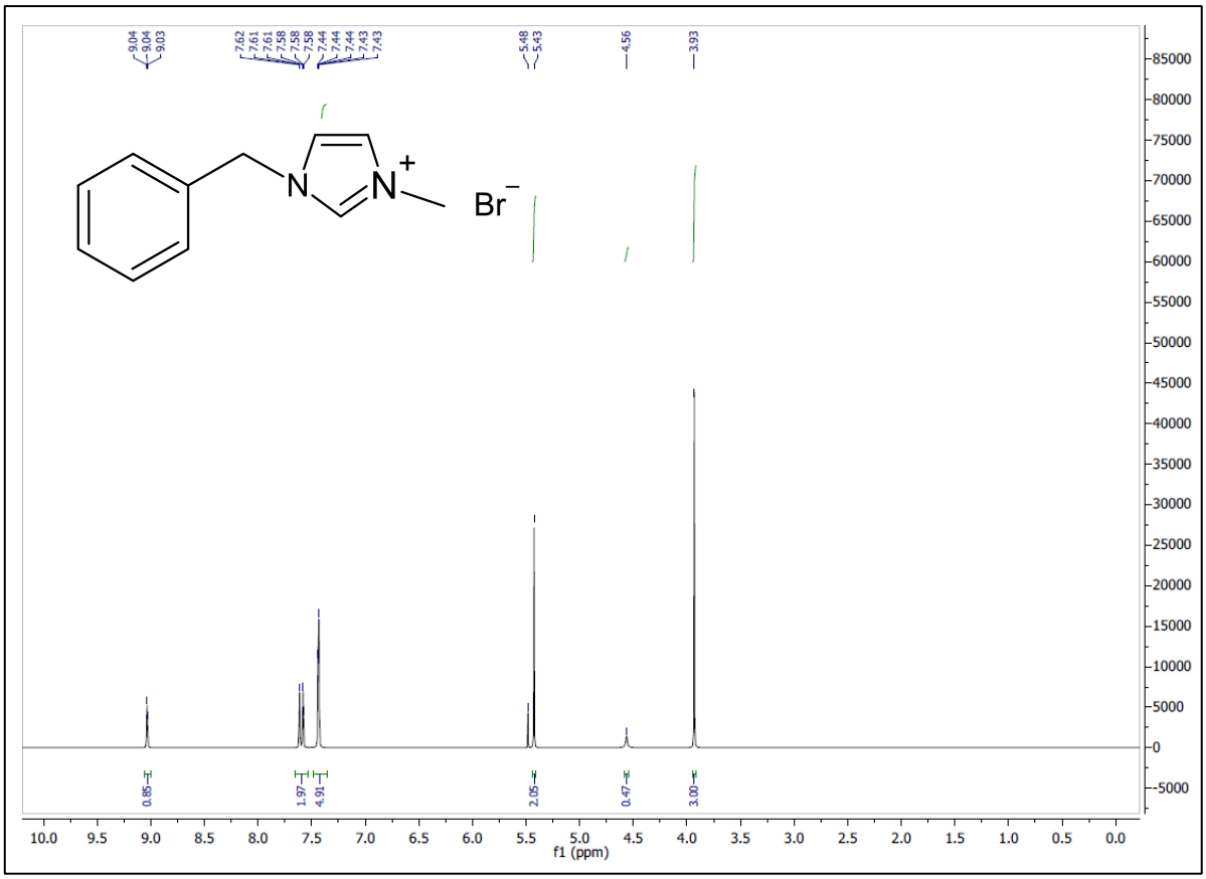
9.04
9.04
9.03
7.62
7.61
7.61
7.58
7.58
7.58
7.44
7.44
7.44
7.43
7.43
5.48
5.43
4.56
3.93
N
N+
Br−
0.85
1.97
4.91
2.05
0.47
3.00
f1 (ppm)

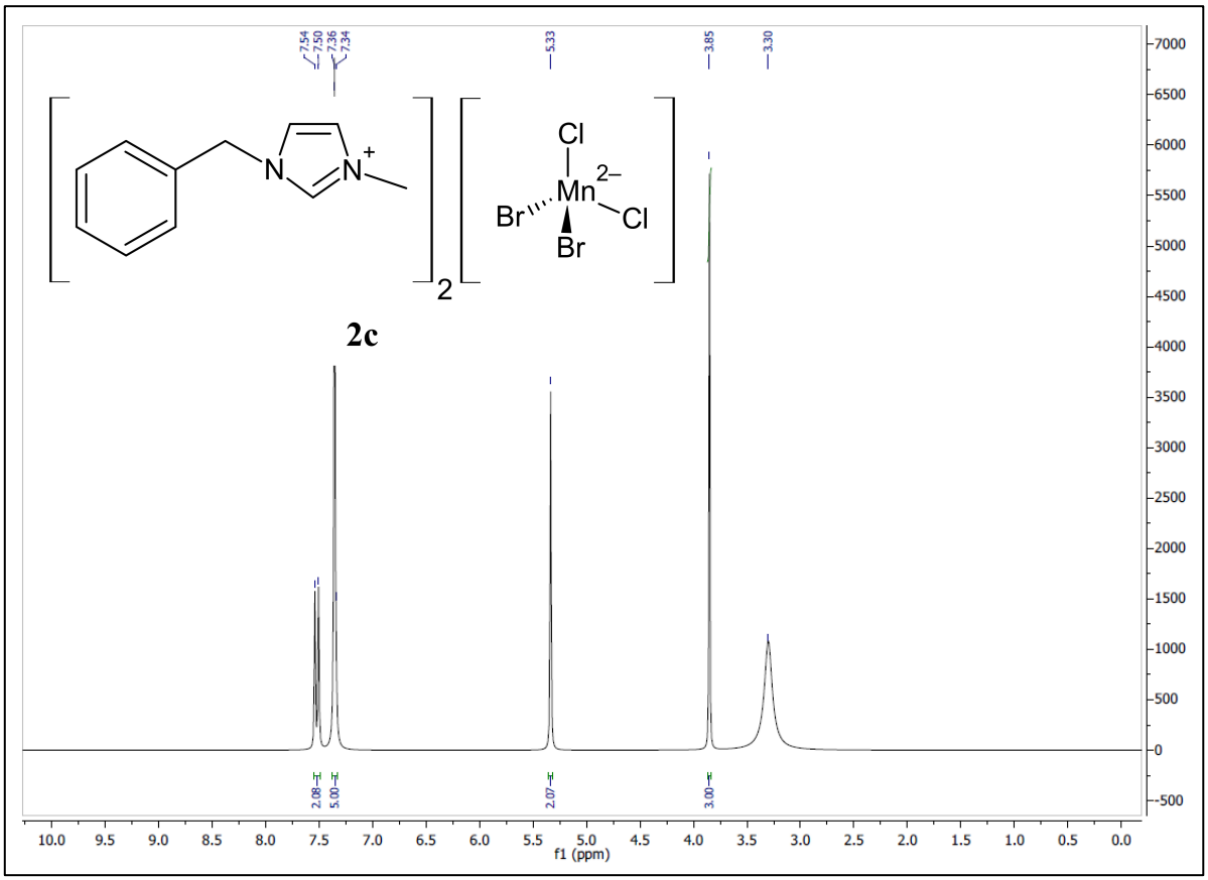
7.54
7.50
7.36
7.34
5.33
3.85
3.30
N
N+
2
Cl
Mn2−
Br
Br
Cl
2c
2.08
5.00
2.07
3.00
f1 (ppm)

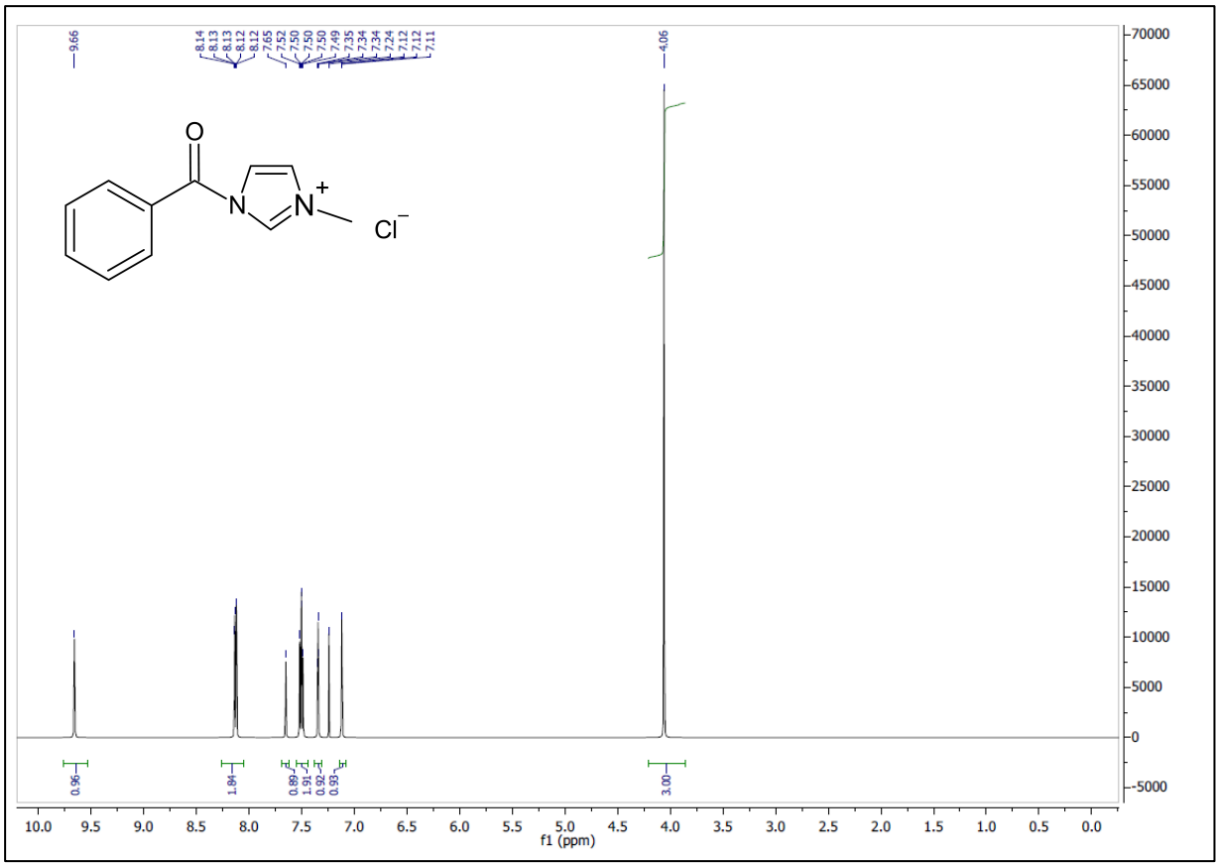
9.66
8.14
8.13
8.12
7.65
7.52
7.50
7.49
7.35
7.34
7.24
7.12
7.11
4.06
O
N
N+
Cl−
0.96
1.84
0.89
1.91
0.92
0.93
3.00
f1 (ppm)

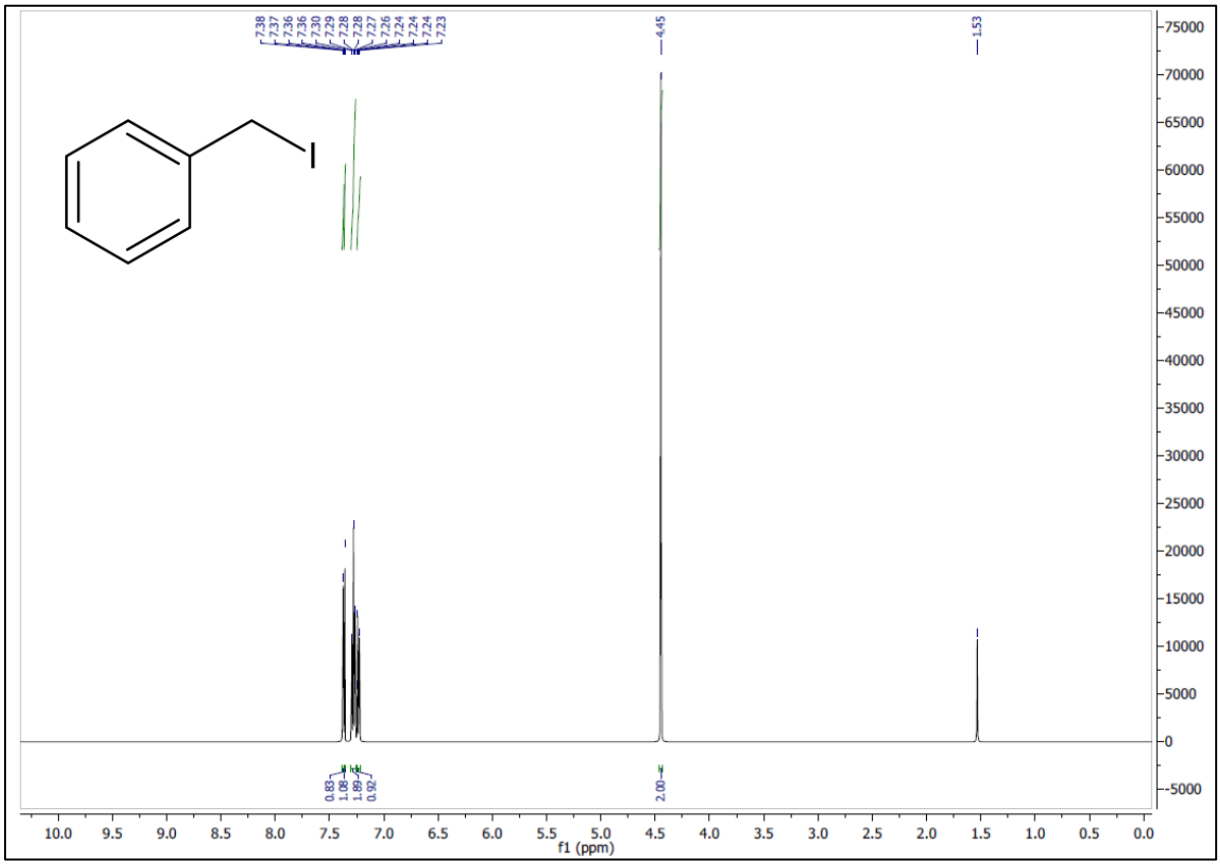
7.38
7.37
7.36
7.30
7.29
7.28
7.27
7.26
7.24
7.24
7.24
7.23
4.45
1.53
I
0.83
1.08
1.89
0.92
2.00
f1 (ppm)

Appendix 4. Details of syntheses for complexes **1a**–**1e**.

Complex, Formula	*M* (g/mol)	[EMIm]X		MnY_2 or $MnY_2 \cdot 4H_2O$		Product		Yield (%)
		m (g)	*n* (mmol)	*m* (g)	*n* (mmol)	*m* (g)	*n* (mmol)	
$[EMIm]_2[MnCl_4]$ (**1a**)	419.08	[EMIm]Cl		$MnCl_2$		0.9654	2.30	100
		0.6742	4.60	0.2899	2.30			
$[EMIm]_2[MnBr_4]$ (**1b**)	596.91	[EMIm]Br		$MnBr_2 \cdot 4H_2O$		0.9876	1.65	101
		0.6267	3.28	0.4698	1.64			
		[EMIm]Br		$MnBr_2 \cdot 4H_2O$		1.4095	2.36	91
		0.9868	5.16	0.7411	2.58			
$[EMIm]_2[MnI_4]$	784.89	[EMIm]I		MnI_2		1.0321	1.31	100
		0.6288	2.64	0.4085	1.32			
$[EMIm]_2[MnBr_2Cl_2]$ (**1c**)	507.98	[EMIm]Br		$MnCl_2$		0.9794	1.93	96
		0.7647	4.00	0.2520	2.00			
$[EMIm]_2[MnCl_2I_2]$ (**1d**)	601.99	[EMIm]Cl		MnI_2		0.9105	1.51	99
		0.4476	3.05	0.4710	1.53			
		[EMIm]I		$MnCl_2$		0.9679	1.61	99
		0.7738	3.25	0.2049	1.63			
$[EMIm]_2[MnBr_2I_2]$ (**1e**)	690.89	[EMIm]I		$MnBr_2 \cdot 4H_2O$		0.6606	0.96	94
		0.4916	2.06	0.2926	1.02			
		[EMIm]I		$MnBr_2 \cdot 4H_2O$		0.7897	1.14	89
		0.6101	2.56	0.3719	1.30			

Appendix 5. ^{1}H NMR and elemental analysis results for complexes **1a**–**1e**.

$[EMIm]_2[MnCl_4]$ (**1a**):

^{1}H NMR (methanol-d_4, 500 MHz) δ 8.85 (s, 1H), 7.56 (s, 1H), 7.48 (s, 1H), 4.18 (q, J = 5.0 Hz, 2H), 3.85 (s, 3H), 1.45 (t, J = 5.0 Hz, 3H) ppm.

Elemental analysis calculated (%): N 13.37, C 34.39, H 5.29; found: N 13.11, C 34.49, H 5.38.

$[EMIm]_2[MnBr_4]$ (**1b**):

^{1}H NMR (methanol-d_4, 500 MHz), 1st batch: δ 8.76 (s, 1H), 7.47 (s, 1H), 7.39 (s, 1H), 4.08 (q, J = 5.0 Hz, 2H), 3.75 (s, 3H), 1.36 (t, J = 5.0 Hz, 3H) ppm; 2nd batch: δ 8.77 (s, 1H), 7.47 (s, 1H), 7.39 (s, 1H), 4.08 (q, J = 5.0 Hz, 2H), 3.75 (s, 3H), 1.36 (t, J = 5.0 Hz, 3H) ppm.

Elemental analysis calculated (%): N 9.39, C 24.15, H 3.71 and calculated for $[EMIm]_2[MnBr_4]\cdot 0.05[EMIm]Br$: N 9.65, C 24.83, H 3.82. Found, 1st batch: N 9.46, C 25.16, H 4.16; found, 2nd batch: N 9.48, C 24.88, H 4.23.

$[EMIm]_2[MnCl_2Br_2]$ (**1c**):

^{1}H NMR (methanol-d_4, 500 MHz) δ 7.51 (s, 1H), 7.43 (s, 1H), 4.13 (q, J = 5.0 Hz, 2H), 3.79 (s, 3H), 1.40 (t, J = 5.0 Hz, 3H) ppm.

Elemental analysis calculated (%): N 11.03, C 28.37, H 4.36; found: N 10.87, C 28.41, H 4.57.

$[EMIm]_2[MnCl_2I_2]$ (**1d**):

^{1}H NMR (methanol-d_4, 500 MHz) δ 8.86 (s, 1H), 7.56 (s, 1H), 7.48 (s, 1H), 4.18 (q, J = 5.0 Hz, 2H), 3.85 (s, 3H), 1.46 (t, J = 5.0 Hz, 3H) ppm.

Elemental analysis calculated (%): N 9.31, C 23.94, H 3.68; found: N 9.06, C 23.87, H 3.75.

$[EMIm]_2[MnBr_2I_2]$ (**1e**):

^{1}H NMR (methanol-d_4, 500 MHz), 1st batch: δ 8.87 (s, 1H), 7.58 (s, 1H), 7.50 (s, 1H), 4.20 (q, J = 5.0 Hz, 2H), 3.87 (s, 3H), 1.48 (t, J = 5.0 Hz, 3H) ppm; 2nd batch: δ 8.90 (s, 1H), 7.59 (s, 1H), 7.51 (s, 1H), 4.21 (q, J = 5.0 Hz, 2H), 3.87 (s, 3H), 1.48 (t, J = 5.0 Hz, 3H) ppm.

Elemental analysis calculated (%): N 8.11, C 20.86, H 3.21 and calculated for $[EMIm]_2[MnBr_2I_2]\cdot 0.05[EMIm]I$: N 8.29, C 21.33, H 3.28. Found, 1st batch: N 8.27, C 21.65, H 3.55; found 2nd batch: N 8.44, C 21.95, H 3.76.

Appendix 6. Single crystal structures of complexes **1c** and **2c**.

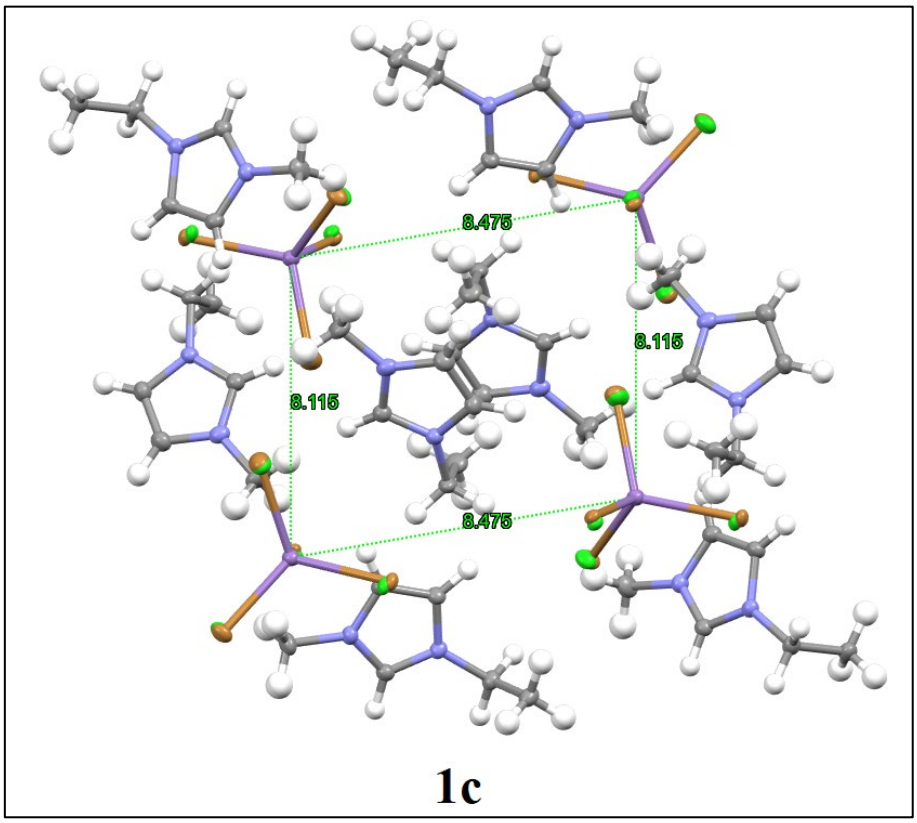

1c

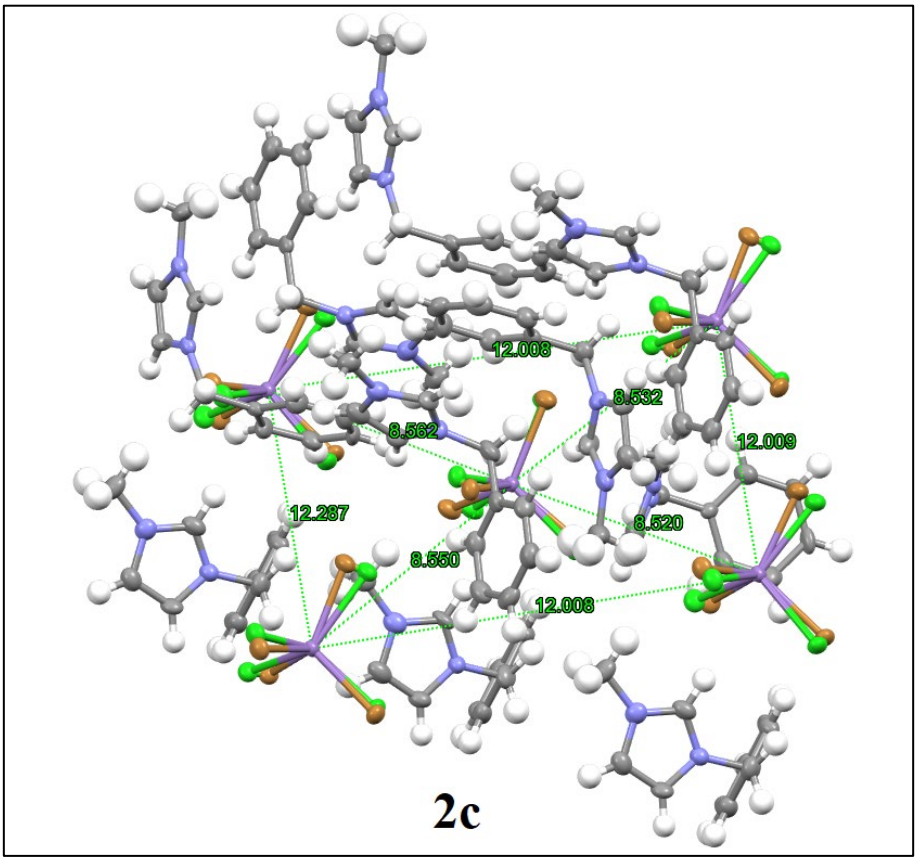

2c

Appendix 7. Details of syntheses of organic precursor salts.

Formula	*M* (g/mol)	1-methylimidazole		R–X		Product		Yield (%)
		V (mL)	*n* (mmol)	*V* (mL)	*n* (mmol)	*m* (g)	*n* (mmol)	
[BnMIm]Br	253.14	0.32	4.01	0.50	4.21	1.12	4.42	110
		0.64	8.03	1.00	8.42	1.97	7.78	97
[BzMIm]Cl	222.67	0.36	4.52	0.55	4.73	1.15	5.16	114
[cHMIm]Cl (DCM)	200.70	0.4	5.02	0.63	5.31	0.35	1.74	35
[cHMIm]Cl (MeCN)		0.4	5.02	0.63	5.31	0.39	1.94	38
[BnMIm]Cl	208.68	0.64	8.03	1.10	9.56	1.39	6.66	83
[BnMIm]I	300.14	0.32	4.01	1.05 g	4.81	1.26	4.20	104

Appendix 8. ^{1}H NMR analysis results for organic precursor salts.

[BnMIm]Br:

^{1}H NMR (methanol-d_4, 500 MHz) δ 9.04 (s, 1H), 7.61 (s, 1H), 7.58 (s, 1H), 7.44 (m, 5H), 5.43 (s, 2H), 3.93 (s, 3H) ppm.

[BzMIm]Cl:

^{1}H NMR (chloroform-d, 500 MHz) δ 9.66 (s, 1H), 8.13 (s, 1H), 8.12 (s, 1H), 7.65 (s, 1H), 7.52 (s, 1H), 7.50 (s, 1H), 7.34 (s, 1H), 7.12 (s, 1H), 4.06 (s, 3H) ppm.

[cHMIm]Cl (originally assumed structure), 1-methylimidazole (real structure):

^{1}H NMR (chloroform-d, 500 MHz) δ 7.28 (s, 1H), 6.91 (s, 1H), 6.75 (s, 1H), 3.55 (s, 3H) ppm.

^{1}H NMR (chloroform-d, 400 MHz, AIST database) δ 7.385 (s, 1H), 7.011 (s, 1H), 6.863 (s, 1H), 3.641 (s, 3H) ppm.

Benzyliodide:

^{1}H NMR (chloroform-d, 500 MHz) δ 7.38 (m, 1H), 7.36 (m, 1H), 7.28 (m, 2H), 7.23 (m, 1H), 4.45 (s, 2H) ppm.

[BnMIm]I:

^{1}H NMR (chloroform-d, 500 MHz) δ 9.87 (m, 1H), 7.46 (m, 3H), 7.37 (m, 1H), 7.32 (m, 3H), 5.52 (s, 2H), 3.99 (s, 3H) ppm.

[BnMIm]Cl:

^{1}H NMR (DMSO-d_6, 500 MHz) δ 9.39 (s, 1H), 7.83 (s, 1H), 7.73 (s, 1H), 7.41 (m, 5H), 5.44 (s, 2H), 3.86 (s, 3H) ppm.

Appendix 9. Details of syntheses for complexes **2a**–**2e** and $[BzMIm]_2[MnBr_2Cl_2]$.

Complex, Formula	*M* (g/mol)	[BnMIm]X		MnY_2 or $MnY_2 \cdot 4H_2O$		Product		Yield (%)
		m (g)	*n* (mmol)	*m* (g)	*n* (mmol)	*m* (g)	*n* (mmol)	
$[BnMIm]_2[MnCl_4]$ (**2a**)	543.20	[BnMIm]Cl		$MnCl_2$		0.8924	1.64	85
		0.8075	3.87	0.2441	1.93			
$[BnMIm]_2[MnBr_4]$ (**2b**)	721.05	[BnMIm]Br		$MnBr_2 \cdot 4H_2O$		0.5645	0.78	86
		0.4608	1.82	0.2615	0.91			
$[BnMIm]_2[MnBr_2Cl_2]$ (**2c**)	632.12	[BnMIm]Br		$MnCl_2$		0.2938	0.46	96
		0.2451	0.97	0.0621	0.49			
		[BnMIm]Br		$MnCl_2$		1.0969	1.73	95
		0.9268	3.66	0.2310	1.83			
$[BnMIm]_2[MnCl_2I_2]$ (**2d**)	726.12	[BnMIm]I		$MnCl_2$		0.5430	0.75	97
		0.4612	1.54	0.0963	0.77			
$[BnMIm]_2[MnBr_2I_2]$ (**2e**)	815.05	[BnMIm]I		$MnBr_2 \cdot 4H_2O$		0.5836	0.72	96
		0.4481	1.49	0.2140	0.75			
$[BzMIm]_2[MnBr_2Cl_2]$	660.07	[BzMIm]Cl		$MnBr_2 \cdot 4H_2O$		0.3457	0.52	92
		0.2541	1.14	0.1628	0.57			

Appendix 10. ^{1}H NMR and elemental analysis results for assumed $[BzMIm]_2[MnCl_2Br_2]$

$[BzMIm]_2[MnCl_2Br_2]$ (assumed), most probably mixture of [BzMIm]Cl and $MnBr_2$:

^{1}H NMR (methanol-d_4, 500 MHz) δ 8.44 (s, 1H), 7.92 (s, 1H), 7.78 (s, 1H), 7.51 (s, 1H) 7.35 (m, 3H), 7.23 (s, 1H), 3.73 (s, 3H) ppm.

Elemental analysis calculated (%): N 8.49, C 40.03, H 3.36; found: N 11.20, C 21.31, H 3.79.

Appendix 11. ^{1}H NMR and elemental analysis results for complexes **2a**–**2e**

$[BnMIm]_2[MnCl_4]$ (**2a**):

^{1}H NMR (methanol-d_4, 500 MHz) δ 7.50 (s, 1H), 7.47 (s, 1H), 7.32 (m, 5H), 5.30 (s, 2H), 3.82 (s, 3H) ppm.

Elemental analysis calculated (%): N 10.31, C 48.64, H 4.82; found: N 10.24, C 48.17, H 4.82.

$[BnMIm]_2[MnBr_4]$ (**2b**):

^{1}H NMR (methanol-d_4, 500 MHz) δ 7.53 (s, 1H), 7.50 (s, 1H), 7.35 (m, 5H), 5.33 (s, 2H), 3.85 (s, 3H) ppm.

Elemental analysis calculated (%): N 7.77, C 36.65, H 3.63 and calculated for $[BnMIm]_2[MnBr_4]\cdot 0.05[BnMIm]Br$: N 7.94, C 37.42, H 3.71; found: N 7.84, C 37.50, H 4.28.

$[BnMIm]_2[MnCl_2Br_2]$ (**2c**):

^{1}H NMR (methanol-d_4, 500 MHz) δ 7.54 (s, 1H), 7.50 (s, 1H), 7.35 (m, 5H), 5.33 (s, 2H), 3.85 (s, 3H) ppm.

Elemental analysis calculated (%): N 8.86, C 41.80, H 4.15; found: N 8.82, C 42.33, H 4.25.

$[BnMIm]_2[MnCl_2I_2]$ (**2d**):

^{1}H NMR (methanol-d_4, 500 MHz) δ 7.59 (s, 1H), 7.55 (s, 1H), 7.40 (m, 5H), 5.38 (s, 2H), 3.90 (s, 3H) ppm.

Elemental analysis calculated (%): N 7.72, C 36.39, H 3.61; found: N 7.62, C 36.77, H 3.62.

$[BnMIm]_2[MnBr_2I_2]$ (**2e**):

^{1}H NMR (methanol-d_4, 500 MHz) δ 7.54 (s, 1H), 7.51 (s, 1H), 7.36 (m, 5H), 5.34 (s, 2H), 3.86 (s, 3H) ppm.

Elemental analysis calculated (%): N 6.87, C 32.42, H 3.22 and calculated for $[BnMIm]_2[MnBr_2I_2]\cdot 0.05[BnMIm]I$: N 7.00, C 33.00, H 3.27; found: N 6.88, C 32.99, H 3.72.

Appendix 12. Melting and thermal degradation onset point determination of **1c** (a) and **2c** (b).

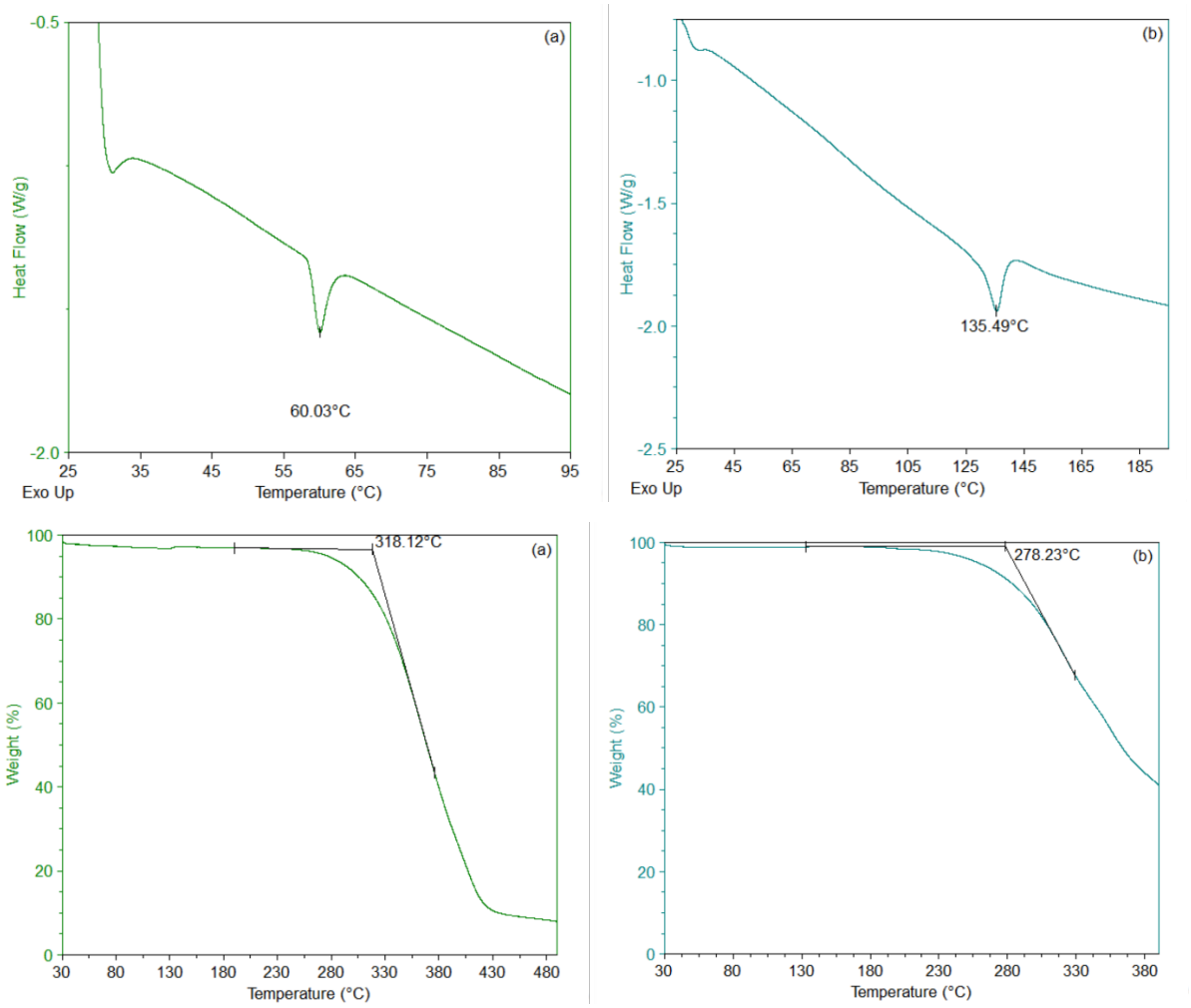

Non-exclusive license to reproduce the thesis and make the thesis public

I, Verner Sääsk (24.02.1998)

(*author's name*)

1. herewith grant the University of Tartu a free permit (non-exclusive license) to use my work,

Design of Highly Luminescent Anionic Manganese(II) Complexes for Application in Organic Light-Emitting Diodes

(*title of thesis*)

supervised by Hou-Hsiu Chou (PhD) and Kaija Põhako-Esko (PhD)

(*supervisor's name*)

2. I grant the University of Tartu the permit to make the thesis specified in point 1 available to the public via the web environment of the University of Tartu, including via the DSpace digital archives, under the Creative Commons licence CC BY NC ND 4.0, which allows, by giving appropriate credit to the author, to reproduce, distribute the work and communicate it to the public, and prohibits the creation of derivative works and any commercial use of the work from **30.05.2024** until expiry of the term of validity of the copyright,

3. I am aware that the author retains the rights specified in points 1 and 2.

4. I confirm that granting the non-exclusive licence does not infringe other persons' intellectual property rights or rights arising from the personal data protection legislation.

Verner Sääsk

Tartu, **23.05.2023**